

Economical model for B -flavour and a_μ anomalies from $\text{SO}(10)$ grand unification

Ufuk Aydemir,^{1,2,*} Tanumoy Mandal,^{3,†} Subhadip Mitra,^{4,‡} and Shoaib Munir^{5,6,§}

¹*Department of Physics, Middle East Technical University, Ankara 06800, Türkiye*

²*Institute of High Energy Physics, Chinese Academy of Sciences, Beijing 100049, P. R. China*

³*Indian Institute of Science Education and Research Thiruvananthapuram, Vithura, Kerala, 695 551, India*

⁴*Center for Computational Natural Sciences and Bioinformatics,*

International Institute of Information Technology, Hyderabad 500 032, India

⁵*East African Institute for Fundamental Research (ICTP-EAIFR), University of Rwanda, Kigali, Rwanda*

⁶*Department of Physics, Faculty of Natural Sciences and Mathematics, St. Olaf College, Northfield, MN 55057, USA*

(Dated: October 1, 2024)

We investigate an $\text{SO}(10)$ grand unification scenario where the complex 10-dimensional scalar multiplet, containing the Standard Model (SM) Higgs boson, resides at the TeV scale altogether. The resulting low-energy model is a 2-Higgs-doublet model augmented with two S_1 -type leptoquarks. The gauge-coupling unification is achieved with only one intermediate scale at which the Pati-Salam gauge group is broken down to the SM. Proton stability is ensured by a discrete symmetry, leftover from the breaking of the $\text{U}(1)_{\text{PQ}}$ global symmetry. The axion corresponding to this broken $\text{U}(1)_{\text{PQ}}$ provides a solution to the strong CP problem, and also serves as an important dark matter candidate. We discuss how the simultaneous explanation for the $R_{D^{(*)}}$ and a_μ anomalies comes about in the model, and investigate some of its phenomenological implications.

Keywords: B -decay anomalies, scalar leptoquark, $\text{SO}(10)$ grand unification, LHC, 2HDM, axions, Peccei-Quinn symmetry, strong CP problem, dark matter

I. INTRODUCTION

During the past few years, several disagreements between particle physics experiments and the SM predictions of the rare B -decays have been reported by the BaBar [1, 2], LHCb [3–7], and Belle [8, 9] collaborations. A pair of such anomalous measurements that has persisted (not without significant fluctuations, though) corresponds to the $R_{D^{(*)}}$ observables, defined as

$$R_{D^{(*)}} = \frac{\text{BR}(B \rightarrow D^{(*)} \tau \nu)}{\text{BR}(B \rightarrow D^{(*)} \ell \nu)}, \quad (1)$$

where $\ell = \{e, \mu\}$, and BR stands for branching ratio. The latest averaged experimental values of these observables read [10]

$$\begin{aligned} R_D &= 0.342 \pm 0.026, \\ R_{D^*} &= 0.287 \pm 0.012 \end{aligned} \quad (2)$$

which exceed the averaged SM predictions, $R_D^{\text{SM}} = 0.298$ and $R_{D^*}^{\text{SM}} = 0.254$, estimated by the Heavy Flavor Averaging Group [11] by more than 3σ (taking into account the R_D - R_{D^*} correlation) [10]. Another persistent collider anomaly is the measurement of the magnetic moment of the muon, a_μ . Its current BNL [12] and FNAL [13] experimental average, $\{116\,592\,059 \pm 22\} \times 10^{-11}$, deviates from $a_\mu^{\text{SM}} = \{116\,591\,810 \pm 43\} \times 10^{-11}$ [14–34] by 5.1σ , so that

$$\Delta a_\mu = \{24.9 \pm 4.8\} \times 10^{-10}. \quad (3)$$

There are many proposed new physics scenarios that could explain these anomalies, mostly introducing particles on an ad-hoc basis. However, a compelling rationale for the consistency of TeV-scale particles with the existing frameworks of ultraviolet (UV)-completion is mostly overlooked. While no such motivation is a requisite in a bottom-up approach, it is nevertheless appealing to search for a UV-compatible picture based on our current understanding of the SM. Motivated by this, we investigate here a low-energy model originating from a grand unified theory (GUT).

The existence of some particles in a GUT framework at the TeV scale could be approached in the context of the splitting of the parent multiplet containing the SM Higgs field into two (or more) mass scales. A large mass-splitting is a well-known problem in supersymmetric and non-supersymmetric GUTs both, and can, quite obviously, be circumvented (at least to some extent) if the companions of the doublet Higgs field in the $\text{SO}(10)$ multiplet also lie at the TeV scale. The null results from the new particle searches at the large hadron collider (LHC), and at the same time the anticipation about its upcoming extended run(s), make the relatively small and economical TeV-scale multiplet, such as a 10-dimensional scalar representation $\mathbf{10}_H$, a rather appealing prospect. This representation ordinarily implies a real multiplet which can contain only the electroweak (EW) Higgs doublet along with a S_1 -type scalar leptoquark, which we generically denote by \tilde{L} henceforth. Such a leptoquark has been extensively studied in the literature [35–54] as a plausible explanation for the $R_{D^{(*)}}$ and the a_μ anomalies, although it has now been realised that a single \tilde{L} cannot explain all

* uaydemir@ihep.ac.cn

† tanumoy@iisertvm.ac.in

‡ subhadip.mitra@iiit.ac.in

§ smunir@eaifr.org

these anomalies simultaneously [47].¹

Extension of the SM by a solo \tilde{L} resulting from a real SO(10) multiplet, $\mathbf{10}_H$, has been studied in Ref. [50] to address only the $R_{D^{(*)}}$ anomalies. The more popular scenario in the literature is the one with the complex(ified) version of the $\mathbf{10}_H$ multiplet [57, 58], which has its advantages in the context of the fermion mass relations and requires less number of large GUT multiplets compared to the real case [59]. The complex multiplet $\mathbf{10}_H$ yields two Higgs doublets along with two \tilde{L} fields, which are assumed to lie at the TeV-scale in our scenario. The fact that TeV-scale 2-Higgs doublet models (2HDMs) are themselves phenomenologically favorable for multiple reasons (see [60] for a review) makes this scenario even more appealing to explore.

The TeV-scale particle content of the model does not lead to gauge-coupling unification at the purported GUT scale, where the masses of the rest of the particles are assumed to lie. Therefore, we follow the common route of inserting a single intermediate stage where the active gauge group is the Pati-Salam group, $SU(4)_C \otimes SU(2)_L \otimes SU(2)_R$, the breaking of which appears to be favored by various phenomenological bounds [61]. In our model, the SO(10) symmetry is thus broken at the unification scale M_U into the Pati-Salam gauge group, which itself subsequently breaks into the SM gauge group at an intermediate energy scale M_{PS} .

Furthermore, a Peccei-Quinn global symmetry, $U(1)_{PQ}$ [62–64], is introduced along with a singlet scalar, which provides the axion that resolves the strong CP problem and constitutes a dark matter (DM) candidate upon acquiring a vacuum expectation value (VEV) [57, 58, 65, 66]. The couplings of the leptoquarks that can potentially lead to proton decay are forbidden by imposing a discrete symmetry, identified with the baryon number, as we will discuss in the next section.

A 2HDM, which the Higgs sector of our low-energy model resembles, can itself explain Δa_μ , albeit in a very narrow parameter space region, due to the presence of a charged scalar, H^\pm [67–92]. It has also been studied as a prospect accommodating the $R_{D^{(*)}}$ anomalies [93], and found to serve the purpose only with additional structure [94–98] (again, in the bottom-up approach). In the model explored in this article, the synergy between the two copies of \tilde{L} augmenting the GUT-inspired 2HDM at the low energy provides a rather natural recipe for explaining these anomalies. Our analysis shows that even in the most minimal scenario of this model, they can indeed be successfully addressed simultaneously.

The rest of the article is organised as follows. In Sec. II we present at length the GUT framework of our interest, as well as the resulting low-energy model. In Sec.

III we overview the model’s parameter space of our interest. This is followed in Sec. IV by the details of the analysis of our low-energy model’s predictions against the experimental data. In Sec. V we discuss some of the phenomenological implications of our model, and in Sec. VI we conclude our findings.

II. THE SO(10) MODEL

A. The UV framework

In the SO(10) framework, each family of the SM fermions, augmented by right-handed neutrinos, resides in a $\mathbf{16}$ spinor-representation. As for the scalar field content responsible for the Yukawa sector, a combination of $\mathbf{10}$, $\mathbf{120}$ and $\mathbf{126}$ representations must be selected, since

$$\mathbf{16} \otimes \mathbf{16} = \mathbf{10} \oplus \mathbf{120} \oplus \mathbf{126} . \quad (4)$$

In this paper, for the UV part, we will adopt the common framework wherein the scalar sector consists of a complex(ified) $\mathbf{10}_H$ and a complex $\mathbf{126}_H$, which is known to yield a realistic Yukawa sector (e.g. fermion mass relations and mixing patterns) as well as a successful see-saw mechanism for the neutrino masses [57, 58, 65].²

In addition to these two multiplets, a $\mathbf{54}_H$ is utilised to break the SO(10) symmetry. Finally, we also have a scalar singlet S , which breaks the $U(1)_{PQ}$ symmetry [62–64], imposed to resolve the strong CP problem, provides a potential DM candidate, and increases the predictivity of the theory by forbidding certain terms in the Lagrangian [57, 58, 65, 66]. The last feature also leads to the so-called Type-II 2HDM along with two leptoquarks at the low energy (see Eq. (15) below), which is the main focus of this paper.

The Yukawa terms are given as

$$\mathcal{L}_Y = \mathbf{16}_F (Y_{10} \mathbf{10}_H + Y_{126} \overline{\mathbf{126}}_H) \mathbf{16}_F + \text{H.c.} , \quad (5)$$

where Y_{10} and Y_{126} are complex matrices, symmetric in the generation space. The $\mathbf{10}_H^*$ term is forbidden by the $U(1)_{PQ}$ symmetry, the assigned charges of which are

$$\begin{aligned} \mathbf{16}_F &\rightarrow e^{i\alpha} \mathbf{16}_F , & \mathbf{10}_H &\rightarrow e^{-2i\alpha} \mathbf{10}_H , \\ \mathbf{126}_H &\rightarrow e^{2i\alpha} \mathbf{126}_H , & S &\rightarrow e^{-4i\alpha} S . \end{aligned} \quad (6)$$

¹ We note here that the 3.1σ deviation previously reported by the LHCb collaboration [55] in the measurement of the $R_{K^{(*)}} \equiv \frac{\text{BR}(B \rightarrow K^{(*)} \mu^+ \mu^-)}{\text{BR}(B \rightarrow K^{(*)} e^+ e^-)}$ observables from their SM prediction of 1.00 ± 0.01 has recently been refuted [56].

² A real $\mathbf{10}_H$, instead of the complex one, is also a phenomenologically viable option [59, 99], although the earlier discussions suggested otherwise [57]. In fact, we utilised in Ref. [50] a version of this SO(10) framework with a real $\mathbf{10}_H$ near the EW scale (and with a different SO(10) scalar content and Yukawa sector), which yields, besides the SM Higgs boson, a single TeV-scale \tilde{L} explaining the $R_{D^{(*)}}$ anomalies. The light complex $\mathbf{10}_H$, which is the case in this paper, yields a much richer structure, enabling us to additionally explain the a_μ anomaly.

The VEV of the $\mathbf{126}_H$ field can only break a linear combination of $U(1)_{B-L}$ and $U(1)_{PQ}$ (and hence the Pati-Salam group) into the SM group. Therefore, in order to obtain the Goldstone boson (axion), the singlet S above has been introduced [100] to break the $U(1)_{PQ}$ alone by acquiring a VEV $\langle S \rangle \equiv M_{PQ} \simeq f_a$, where f_a is the axion decay constant. This symmetry could also be broken by $\langle \mathbf{10}_H \rangle$, similarly to the original axion model [62–64], but in that case one would obtain $M_{PQ} = M_{EW}$, which has long been ruled out [101, 102] (see also Ref. [103] for a review). The scale M_{PQ} is independent of the unification scale M_U , and its value can be chosen in accordance with the axion phenomenology. In Ref. [58] $M_{PQ} \sim 10^{10} - 10^{12}$ GeV was selected in a full numerical fit of the model parameters, which is consistent with the current constraints, and yields the axion mass $m_a \sim 10 - 200$ μeV , making it a suitable candidate for the DM of the Universe.

The Pati-Salam and SM decompositions of the $\mathbf{10}_H$ are given as

$$\begin{aligned} \mathbf{10} &= \Phi(1, 2, 2)_{422} \oplus \Xi(6, 1, 1)_{422} \\ &= \phi_1 \left(1, 2, \frac{1}{2}\right)_{321} \oplus \phi_2 \left(1, 2, -\frac{1}{2}\right)_{321} \\ &\quad \oplus \xi_1 \left(3, 1, -\frac{1}{3}\right)_{321} \oplus \xi_2 \left(\bar{3}, 1, \frac{1}{3}\right)_{321}, \quad (7) \end{aligned}$$

where the subscripts denote the corresponding gauge group, and we have set $Q = I_3 + Y$. H_1 and H_2 are the up- and down-type Higgs doublets, as in the 2HDM that will be a part of our low-energy model. The $\mathbf{126}$ decomposes as

$$\begin{aligned} \mathbf{126} &= \Delta_L(10, 3, 1)_{422} \oplus \Delta_R(\bar{10}, 1, 3)_{422} \\ &\quad \oplus \Sigma(15, 2, 2)_{422} \oplus \Xi'(6, 1, 1)_{422}. \quad (8) \end{aligned}$$

The breaking sequence of the gauge symmetry of the model is schematically given as

$$SO(10) \xrightarrow[\langle \mathbf{54}_H \rangle]{M_U} G_{422D} \xrightarrow[\langle \mathbf{126}_H \rangle]{M_{PS}} G_{321}(\text{SM}) \xrightarrow[\langle \mathbf{10}_H \rangle]{M_Z} G_{31}, \quad (9)$$

where we have used the notation

$$\begin{aligned} G_{422D} &\equiv SU(4)_C \otimes SU(2)_L \otimes SU(2)_R \otimes D, \\ G_{321} &\equiv SU(3)_C \otimes SU(2)_L \otimes U(1)_Y, \\ G_{31} &\equiv SU(3)_C \otimes U(1)_Q. \quad (10) \end{aligned}$$

Here D denotes the D -parity, or left-right symmetry, a \mathbb{Z}_2 symmetry that maintains the complete equivalence of the left and right sectors [104, 105]. The first stage of the spontaneous symmetry-breaking occurs through the Pati-Salam singlet in $\mathbf{54}_H$ acquiring a VEV at the unification scale M_U . This singlet is even under D parity and, therefore, the resulting symmetry group is G_{422D} .³

In the second step, the breaking of the G_{422D} into the SM gauge group G_{321} is realised when the SM singlet, contained in $\Delta_R(\bar{10}, 1, 3)_{422}$ of $\mathbf{126}_H$, acquires a VEV at the energy scale M_{PS} , which also yields a Majorana mass for the right-handed neutrino. In the last stage of the symmetry-breaking, the SM doublets contained in $\Phi(1, 2, 2)_{422}$ of the complex $\mathbf{10}_H$ acquire a VEV at the EW scale. Additionally, the SM doublets in the $\Sigma(15, 2, 2)_{422}$ of the $\mathbf{126}_H$ acquire VEVs as well, with their contributions correcting the otherwise problematic fermion mass and mixing relations, to yield a realistic model. Since these contributions are controlled by the factor M_{PS}/M_{Σ} , the mass of $\Sigma(15, 2, 2)_{422}$ (M_{Σ}) should be around the Pati-Salam breaking scale, $M_{PS} \equiv \langle \mathbf{126}_H \rangle$, for them to have the desired magnitudes [57, 58]. The fermion mass matrices for the up- and down-type quarks, charged leptons, Dirac neutrinos, and Majorana neutrinos are given as

$$\begin{aligned} M_U &= v_{10}^u Y_{10} + v_{126}^u Y_{126}, \quad M_D = v_{10}^d Y_{10} + v_{126}^d Y_{126} \\ M_E &= v_{10}^d Y_{10} - 3v_{126}^d Y_{126}, \\ M_{\nu_D} &= v_{10}^u Y_{10} - 3v_{126}^u Y_{126}, \quad M_{\nu_M} = \sigma Y_{126}, \quad (11) \end{aligned}$$

where v_{10}^u, v_{10}^d are the VEVs of the two complex doublets in the (complex) $\mathbf{10}_H$, v_{126}^u and v_{126}^d are VEVs of the two complex doublets in $\Sigma(15, 2, 2)_{422}$ of the $\mathbf{126}_H$, while σ denotes the VEV of the SM singlet in $\mathbf{126}_H$.

The potential term, $\propto \mathbf{126}_H \cdot \bar{\mathbf{126}}_H \cdot \mathbf{126}_H \cdot \mathbf{10}_H$ responsible for the above fixing, as well as the potential terms corresponding to the singlet field S , which breaks the $U(1)_{PQ}$ symmetry, introduce mixing in the mass matrices. Therefore, the doublets $(1, 2, \frac{1}{2})_{321}$ and triplets $(3, 1, -\frac{1}{3})_{321}$ in $\mathbf{10}_H$ and $\mathbf{126}_H$ mix among their own kinds. A fine-tuning of the parameters appearing in the mixing matrices is commonly adopted to ensure that, out of this combination, the masses of only the SM doublets lie at the EW scale, while all the other doublets and triplets, which can induce proton-decay-mediating interactions, remain at the intermediate and the GUT-breaking scales. As noted earlier, we deviate from the last assumption in this paper.

The mass-separation of the components of a large multiplet is generally known as the splitting problem in the literature. The mass terms of the doublets and triplets in a given $\mathbf{10}_H$ are identified with the same parameters, up to $\mathcal{O}(1)$. The relevant potential terms are

SO(10) symmetry, in which case the D -parity will also be broken at M_U , since the Pati-Salam singlet in $\mathbf{210}_H$ is odd under it. We however choose to use the $\mathbf{54}_H$ in order for our model to align with the one in Ref [58].

³ A $\mathbf{210}_H$, instead of the $\mathbf{54}_H$, can also be used to break the

given as [58]

$$\begin{aligned}\mathcal{V} = & m^2 |\mathbf{10}_H|^2 + \eta' \mathbf{10}_H^* \cdot \mathbf{54}_H \cdot \mathbf{10}_H + \frac{\eta_0}{2} \mathbf{54}_H^2 |\mathbf{10}_H|^2 \\ & + \eta_2 \mathbf{10}_H^* \cdot \mathbf{54}_H \cdot \mathbf{54}_H \cdot \mathbf{10}_H + \chi |\mathbf{10}_H|^2 |S|^2 \\ & + \frac{\gamma_1}{4!} \mathbf{10}_H^* \cdot \overline{\mathbf{126}}_H \cdot \mathbf{126}_H \cdot \mathbf{10}_H \\ & + \frac{\gamma_2}{4!} \mathbf{10}_H^* \cdot \mathbf{126}_H \cdot \overline{\mathbf{126}}_H \cdot \mathbf{10}_H \\ & + \eta_1 \mathbf{126}_H \cdot \overline{\mathbf{126}}_H \cdot \mathbf{126}_H \cdot \mathbf{10}_H \dots\end{aligned}\quad (12)$$

$\mathbf{54}_H$ acquires a VEV

$$\langle \mathbf{54}_H \rangle = \text{diag}(-2/5 \mathbf{I}_{6 \times 6}, 3/5 \mathbf{I}_{4 \times 4}) \omega, \quad (13)$$

breaking the SO(10) symmetry, where $\omega \sim M_U$. The VEVs of the singlets in $\mathbf{54}_H$ and $\mathbf{126}_H$ are given as $\langle \mathbf{1}_{54} \rangle = -\sqrt{12/5} \omega$ and $\langle \mathbf{1}_{126} \rangle = \sigma/\sqrt{2} (\simeq M_{\text{PS}})$, and the VEV of S , which itself is a singlet, becomes $\langle S \rangle = v_s/\sqrt{2} \simeq M_{\text{PQ}} \simeq f_a$. The diagonal terms in the mass-squared matrices of the doublets and triplets of $\mathbf{10}_H$ are given as [58]

$$\begin{aligned}M_{\xi_1}^2 &= -\frac{2}{5} \eta' \omega + \frac{6}{5} \eta_0 \omega^2 + \frac{4}{25} \eta_2 \omega^2 + \gamma_1 \sigma^2 + \frac{1}{2} \chi v_s^2 + m^2, \\ M_{\xi_2}^2 &= -\frac{2}{5} \eta' \omega + \frac{6}{5} \eta_0 \omega^2 + \frac{4}{25} \eta_2 \omega^2 + \gamma_2 \sigma^2 + \frac{1}{2} \chi v_s^2 + m^2, \\ M_{\phi_1}^2 &= \frac{3}{5} \eta' \omega + \frac{6}{5} \eta_0 \omega^2 + \frac{9}{25} \eta_2 \omega^2 + \gamma_1 \sigma^2 + \frac{1}{2} \chi v_s^2 + m^2, \\ M_{\phi_2}^2 &= \frac{3}{5} \eta' \omega + \frac{6}{5} \eta_0 \omega^2 + \frac{9}{25} \eta_2 \omega^2 + \gamma_2 \sigma^2 + \frac{1}{2} \chi v_s^2 + m^2.\end{aligned}\quad (14)$$

The similarity of these terms makes it difficult to split the masses of the members of the multiplet, keeping a doublet light and others at the GUT scale. The mixing with other doublets and triplets, introduced by the η_1 term in Eq. (12) could ameliorate the splitting problem through fine-tuning. Instead, we adopt the picture that whatever mechanism keeps the Higgs doublet light brings other members of the $\mathbf{10}_H$ down to the TeV scale even after the mixing. Note that we still have the seemingly fine-tuned situation but assume that $\mathbf{10}_H$ remains light altogether. We deal with the issue of proton stability through a discrete symmetry to forbid the diquark couplings of our light leptoquarks, as will be mentioned in the next section.

To sum up, we assume that the choice of parameters that keeps one of the doublets at the EW scale also brings the masses of the other components of the complex $\mathbf{10}_H$, *i.e.*, the other Higgs doublet and the two leptoquarks, down to around the same scale. From a minimalist point of view, it is therefore conceivable that the elements necessary to resolve all the anomalies persisting in the experimental data come from a multiplet that resides altogether at the TeV scale. The picture presented in this paper hence originates from an absence of large splitting of the doublet-triplet mass parameters within a multiplet. It, therefore, constitutes a good motivation to keep the entire complex $\mathbf{10}_H$ light, providing a rationale for the existence of new physics around the TeV scale window in the SO(10) framework.

B. The Lagrangian at low energy

The fields with the same quantum numbers as the two Higgs doublets and the two S_1 -type leptoquarks, given in Eq. (7), are denoted in the low-energy Lagrangian below as H_1 and H_2 , and \tilde{L}_1 and \tilde{L}_2 , respectively.⁴ Thus, at the TeV scale, we effectively have a 2HDM augmented by two leptoquarks. For this model to be phenomenologically consistent though, we have to address the problem of the possible decay of the proton via our leptoquarks. The proton stability, in general, could be ensured through various symmetry mechanisms such as the utilisation of a U(1) symmetry [106, 107] or a discrete symmetry [38]. The relevant operators could also be suppressed by mechanisms such as the one discussed in Ref. [108], or they could be completely forbidden for geometrical reasons [45].

In our framework, proton stability is ensured by a \mathbb{Z}_2 symmetry, which is commonly introduced in an ad-hoc manner (see for instance Refs. [38, 50]). However, the U(1)_{PQ} symmetry in our scenario offers a more compelling, and arguably less artificial, alternative. The required discrete symmetry might be a leftover one from the breaking of the U(1)_{PQ}, and has previously been identified as $(-1)^{3B}$ [109], with B being the baryon number. We impose that this symmetry is valid in our framework as well. The corresponding charges are then given as $(q, \tilde{L}_1, \tilde{L}_2) \rightarrow (-q, -\tilde{L}_1, -\tilde{L}_2)$. The rest of the SM particle content is not charged under this symmetry. Therefore, the diquark couplings of the leptoquarks are forbidden and the proton stability is not a concern in the perturbative framework.

In a 2HDM, the coupling of both the Higgs fields to the SM fermions can lead to flavour-changing neutral currents. To avoid these, the most general approach taken is to enforce a \mathbb{Z}_2^H symmetry on the Lagrangian, so that each type of fermions only couples to one of the doublets [110, 111]. This leads to ‘Types’ I-IV of the 2HDM. In our scenario, the 2HDM (augmented by two leptoquarks) that automatically arises from the SO(10) Lagrangian given in Eq. (5), is of the Type II, wherein the H_2 couples only to the u -type quarks, while H_1 couples to the d -type quarks and the charged leptons. In other words, the \mathbb{Z}_2^H symmetry principle corresponding to the Type-II 2HDM is naturally satisfied. Therefore, the Lagrangian relevant for our phenomenological analysis is given by

$$\begin{aligned}\mathcal{L}_S^Y &\supset (\mathbf{\Lambda}_{q\ell}^{1L} \bar{Q}^c i \tau_2 L + \mathbf{\Lambda}_{q\ell}^{1R} \bar{u}_R^c e_R) \tilde{L}_1^* \\ &\quad + (\mathbf{\Lambda}_{q\ell}^{2L} \bar{Q}^c i \tau_2 L + \mathbf{\Lambda}_{q\ell}^{2R} \bar{u}_R^c e_R) \tilde{L}_2 + \text{H.c.},\end{aligned}\quad (15)$$

$$\begin{aligned}\mathcal{L}_H^Y &\supset \bar{Q} (Y_1^d H_1) d_R + \bar{Q} (Y_2^u \tilde{H}_2) u_R \\ &\quad + \bar{L} (Y_1^e H_1) e_R + \bar{L} (Y_2^e \tilde{H}_2) \nu_R + \text{H.c.},\end{aligned}\quad (16)$$

⁴ We will re-denote the physical leptoquark states after mass-mixing at the TeV scale by Q_1 and Q_2 in Sec. III.

where Q and L are the SM quark and lepton doublets (of a given family), respectively, $\mathbf{\Lambda}_{q\ell}^{iL/iR}$ are the leptoquark coupling matrices in flavour space, and $\psi^c = C\bar{\psi}^T$ are charge-conjugate spinors. Note also that the inclusion of the $\tilde{L}_{1,2}$ can affect the stability of the EW vacuum via loop effects [112].

The leptoquark-Higgs coupling terms in the potential are given as

$$-\mathcal{L}_{SH}^P \supset \lambda_{11}|\tilde{L}_1|^2|H_1|^2 + \lambda_{12}|\tilde{L}_1|^2|H_2|^2 + \lambda_{21}|\tilde{L}_2|^2|H_1|^2 + \lambda_{22}|\tilde{L}_2|^2|H_2|^2, \quad (17)$$

while the rest of the (CP-conserving) potential reads

$$\begin{aligned} -\mathcal{L}^P \supset & \bar{M}_1^2|\tilde{L}_1|^2 + \bar{M}_2^2|\tilde{L}_2|^2 - [\bar{M}_{12}^2\tilde{L}_1^\dagger\tilde{L}_2 + \text{H.c.}] \\ & + M_1^2|H_1|^2 + M_2^2|H_2|^2 - [M_{12}^2H_1^\dagger H_2 + \text{H.c.}] \\ & + \frac{1}{2}\bar{\lambda}_1(\tilde{L}_1^\dagger\tilde{L}_1)^2 + \frac{1}{2}\bar{\lambda}_2(\tilde{L}_2^\dagger\tilde{L}_2)^2 \\ & + \bar{\lambda}_3(\tilde{L}_1^\dagger\tilde{L}_1)(\tilde{L}_2^\dagger\tilde{L}_2) + \bar{\lambda}_4(\tilde{L}_1^\dagger\tilde{L}_2)(\tilde{L}_2^\dagger\tilde{L}_1) \\ & + \left[\frac{1}{2}\bar{\lambda}_5(\tilde{L}_1^\dagger\tilde{L}_2)^2 + \text{H.c.} \right] \\ & + \frac{1}{2}\lambda_1(H_1^\dagger H_1)^2 + \frac{1}{2}\lambda_2(H_2^\dagger H_2)^2 \\ & + \lambda_3(H_1^\dagger H_1)(H_2^\dagger H_2) + \lambda_4(H_2^\dagger H_2)(H_1^\dagger H_1) \\ & + \left[\frac{1}{2}\lambda_5(H_1^\dagger H_2)^2 + \text{H.c.} \right]. \end{aligned} \quad (18)$$

Evidently, the Lagrangian given in Eq. (15) should be understood in the effective field theory context. The Higgs and leptoquark couplings in this TeV-scale Lagrangian are induced from the original SO(10) Yukawa couplings. Each of these Yukawa couplings is generated by a linear combination of the unification-scale operators, and gets modified due to the mixing effects induced by the scalar fields' Yukawa couplings to the three chiral families of $\mathbf{16}_F$. It is indeed this rich structure that enables the realisation of a fermion mass spectrum consistent with that of the SM expected at the unification scale [58]. The modification to the renormalisation group (RG) running of the SM Yukawa couplings due to the inclusion of $\mathbf{\Lambda}_{L/R}$ does not lead to substantial changes in this mass spectrum, as discussed in the next section, and hence the main message of [58] is valid in our case as well.

C. Gauge coupling unification

The new particle content at the TeV scale does not lead to the unification of the SM gauge couplings directly, as can be easily verified from the usual formalism given below. We, therefore, adopt the scheme of gauge-coupling unification with a single intermediate step of breaking the Pati-Salam symmetry into the SM group at the scale M_{PS} , as detailed earlier.

For the purpose of our analysis, the one-loop RG running is sufficient. The formalism of this running for the

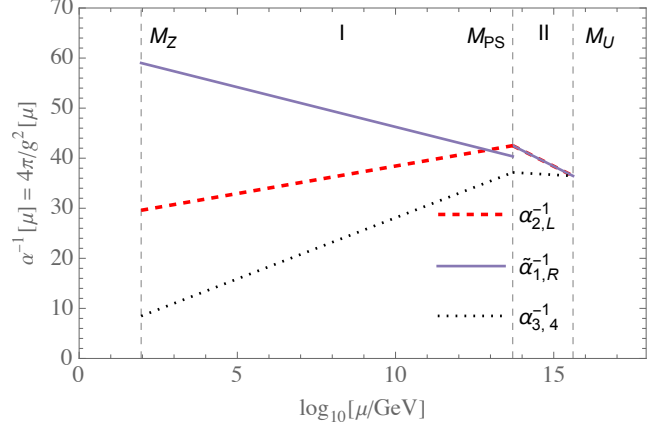


FIG. 1. Running of the gauge couplings. Note that $\tilde{\alpha}_1^{-1} \equiv \frac{3}{5}\alpha_1^{-1}$. The discontinuity at M_{PS} is due to the boundary conditions given in Eq. (A5).

gauge symmetry-breaking sequence shown in Eq. (9) is given in the Appendix A. The scalar content and the RG coefficients in the corresponding energy intervals are given in Table II C, where we label the energy intervals in between the breaking scales $[M_Z, M_{PS}]$ and $[M_{PS}, M_U]$ as

$$\begin{aligned} \text{I} & : [M_Z, M_{PS}], \quad G_{321}(\text{SM}), \\ \text{II} & : [M_{PS}, M_U], \quad G_{422D}. \end{aligned} \quad (19)$$

The central values of the low-energy parameters, used as the boundary conditions in the RG running (in the $\overline{\text{MS}}$ scheme) [113], are $\alpha^{-1} = 127.95$, $\alpha_s = 0.118$, and $\sin^2 \theta_W = 0.2312$ at $M_Z = 91.2 \text{ GeV}$, which translate to $g_1 = 0.357$, $g_2 = 0.652$, and $g_3 = 1.219$. As usual, the coupling constants are all required to remain in the perturbative regime during the evolution from M_Z to M_U . Thus, once the RG coefficients in each interval are specified, the scales M_U and M_{PS} , along with the value of α_U , are uniquely determined through Eqs. (A5) and (A6). This yields

$$\begin{aligned} \log_{10} \left(\frac{M_U}{\text{GeV}} \right) &= 15.6, \quad \log_{10} \left(\frac{M_{PS}}{\text{GeV}} \right) = 13.7, \\ \alpha_U^{-1} &= 36.5, \end{aligned} \quad (20)$$

and the unification of the couplings is displayed in Fig. 1.⁵

As mentioned previously, the proton-decay-mediating couplings of the \tilde{L}_1 are \tilde{L}_2 are forbidden by an assumed discrete symmetry. However, we do not make

⁵ The energy scales found in Eq. (20) are the same as the ones in the model studied in Ref. [50]. This is because, although the RG coefficient a_i are different in each energy interval for the two models, their combinations entering in the Eq. (A5), which determines the energy scales, turn out to be the same, which is not the case for α_U^{-1} and the corresponding Eq. (A6).

Interval	Scalar content for model	RG coefficients
II	$\Phi(1, 2, 2), \Xi(6, 1, 1),$ $\Sigma(15, 2, 2), \Delta_R(\overline{10}, 1, 3),$ $\Delta_L(10, 3, 1)$	$[a_4, a_L, a_R] = \left[1, \frac{26}{3}, \frac{26}{3}\right]$
I	$\phi_1(1, 2, \frac{1}{2})_{321}, \xi_1(3, 1, -\frac{1}{3})_{321}$ $\phi_2(1, 2, -\frac{1}{2})_{321}, \xi_2(\overline{3}, 1, \frac{1}{3})_{321}$	$[a_3, a_2, a_1] = \left[\frac{-20}{3}, -3, \frac{65}{9}\right]$

TABLE I. The scalar content and the RG coefficients in the energy intervals I and II.

any assumptions regarding the other potentially dangerous relevant operators. Thus, it is necessary to inspect whether the predictions given in Eq. (20) are compatible with the current experimental bounds. The most recent and stringent bound on the lifetime of the proton is $\tau_p^{\text{obs}} > 1.6 \times 10^{34}$ years [115]. In our model, the proton-decay can also potentially be mediated by the super-heavy gauge bosons residing in the **45** adjoint representation of the SO(10). For the corresponding operators, $\tau_p \sim M_U^4/m_p^5\alpha_U^2$ [116], where m_p is the proton mass. We obtain $\tau_p \sim 10^{34}$ years, which is consistent with the observation up to $O(1)$. Additionally, the scale M_{PS} determines the expected mass values for the proton-decay-mediating color triplets. A naive analysis [61] shows that the current bounds on the τ_p require $M_{\text{PS}} \gtrsim 10^{11}$ GeV, again consistent with the results given in Eq. (20).

III. LOW-ENERGY PARAMETERS AND OBSERVABLES

From Eqs. (15)-(18), we collect the complete set of free parameters of the model as

$$\begin{aligned} &\{\Lambda_{q\ell}^{1L}, \Lambda_{q\ell}^{1R}, \Lambda_{q\ell}^{2L}, \Lambda_{q\ell}^{2R}, Y_1^d, Y_2^u, Y_1^e, Y_2^\nu, \\ &\lambda_{11}, \lambda_{12}, \lambda_{21}, \lambda_{22}, \bar{M}_1^2, \bar{M}_2^2, \bar{M}_{12}^2, \\ &M_1^2, M_2^2, M_{12}^2, \bar{\lambda}_{1\dots 5}, \lambda_{1\dots 5}\}. \end{aligned} \quad (21)$$

After EW symmetry-breaking, the scalar doublets H_1 and H_2 are defined in terms of their respective VEVs v_1 and v_2 , the physical Higgs states h, H, A and H^\pm , and the Goldstone bosons G and G^\pm , as

$$H_1 = \frac{1}{\sqrt{2}} \begin{pmatrix} \sqrt{2}(G^+c_\beta - H^+s_\beta) \\ v_1 - hs_\alpha + Hc_\alpha + i(Gc_\beta - As_\beta) \end{pmatrix}, \quad (22)$$

$$H_2 = \frac{1}{\sqrt{2}} \begin{pmatrix} \sqrt{2}(G^+s_\beta + H^+c_\beta) \\ v_2 + hc_\alpha + Hs_\alpha + i(Gs_\beta + Ac_\beta) \end{pmatrix}, \quad (23)$$

where c_x and s_x stand for $\cos(x)$ and $\sin(x)$, respectively, with β ($\equiv \tan^{-1}[v_1/v_2]$) and α being the angles rotating the CP-odd and CP-even interaction states, respectively, into physical Higgs states.

As a result, the bare masses M_1 and M_2 can be replaced by v_1 and v_2 using the tadpole conditions for the Higgs potential. In addition, the Higgs quartic couplings $\lambda_{1\dots 5}$ can be traded for the physical masses of the Higgs bosons (m_h, m_H, m_A , and m_{H^\pm}) and the mixing parameter $s_{\beta-\alpha} \equiv \sin(\beta - \alpha)$ as inputs. The Yukawa couplings of the four Higgs bosons are then calculated in the Type-II 2HDM in terms of the mixing angles as

$$\begin{aligned} Y_h^u &= g_u \frac{c_\alpha}{s_\beta}, \quad Y_h^{d/\ell} = -g_{d/\ell} \frac{s_\alpha}{c_\beta}, \\ Y_H^u &= g_u \frac{s_\alpha}{s_\beta}, \quad Y_H^{d/\ell} = g_{d/\ell} \frac{c_\alpha}{c_\beta}, \\ Y_A^u &= \frac{g_u}{t_\beta}, \quad Y_A^{d/\ell} = g_{d/\ell} t_\beta, \end{aligned}$$

where $t_\beta \equiv \tan \beta$, and $g_f = m_f/v$, with $v = \sqrt{v_1^2 + v_2^2}$.

At least one of the Higgs bosons in our model ought to have its mass and Yukawa couplings consistent with the one observed at the LHC. We identify it with the lighter of the two neutral scalars, by fixing $m_h = 125$ GeV and $s_{\beta-\alpha} = 1.0$. The latter corresponds to the so-called alignment limit [117] of the Type-II 2HDM, wherein the h has exactly SM-like couplings to the gauge bosons, since $g_h^V \propto s_{\beta-\alpha}$, while $g_H^V \propto c_{\beta-\alpha}$. In order that the Higgs sector is consistent with the direct search exclusion limits from the LHC, we fixed $M_{12}^2 = (150 \text{ GeV})^2$, $t_\beta = 12$, and $m_H = m_A = m_{H^\pm} = 1 \text{ TeV}$. To ensure this consistency, we nevertheless tested this Higgs sector parameter with the **HiggsBounds-v5.10.0** [118] program. Equal masses of all the heavy Higgs states also imply that the oblique parameters S, T , and U are always ~ 0 , and hence satisfy the 95% confidence level (CL) limits from the 2024 PDG report [113].

As for the leptoquark sector, since this analysis is focused specifically on its contributions to the anomalous flavour observables rather than its own collider phenomenology, we assume the minimal low-energy scenario. We set $\bar{M}_{12}^2 = \bar{\lambda}_1 = \bar{\lambda}_2 = \bar{\lambda}_3 = \bar{\lambda}_4 = \bar{\lambda}_5 = 0$, so that $\bar{M}_1^2 = m_{Q_1}^2$ and $\bar{M}_2^2 = m_{Q_2}^2$, where Q_1 (Q_2) is the lighter (heavier) of the two leptoquark mass eigenstates. This also allows us to retain the leptoquark couplings $\Lambda_{q\ell}^{1L}, \Lambda_{q\ell}^{1R}, \Lambda_{q\ell}^{2L}$, and $\Lambda_{q\ell}^{2R}$ as the input free-parameters at the EW scale, but we switch their respective notations to $\lambda_{q\ell}^{Q_1L}, \lambda_{q\ell}^{Q_1R}, \lambda_{q\ell}^{Q_2L}$, and $\lambda_{q\ell}^{Q_2R}$ from here onward.

The contribution of the S_1 -type \tilde{L} to a_μ can be approximated by [119]

$$\Delta a_\mu \simeq -\frac{N_c}{8\pi^2} \frac{m_t m_\mu}{m_{\tilde{L}}^2} V_{tb} \lambda_{32}^{\tilde{L}L} \lambda_{32}^{\tilde{L}R} \left[\frac{7}{6} + \frac{2}{3} \log x_t \right], \quad (24)$$

where m_t (m_μ) is the top (muon) mass, $x_t = m_t^2/m_{\tilde{L}}^2$, and V_{tb} is the relevant CKM matrix element. Unlike a_μ , the observables

$$\begin{aligned} R_D &\simeq R_D^{\text{SM}} \left(|1 + C_V^L|^2 + 1.09 |C_S^L|^2 + 0.75 |C_T^L|^2 \right. \\ &\quad + 1.54 \text{Re}[(1 + C_V^L)(C_S^L)^*] \\ &\quad + 1.04 \text{Re}[(1 + C_V^L)(C_T^L)^*] + 1.5 \text{Re}(C_{RL}^{\tau 3} + C_{LL}^{\tau 3}) \\ &\quad \left. + 1.0 |C_{RL}^{\tau 3} + C_{LL}^{\tau 3}|^2 \right), \end{aligned} \quad (25)$$

and

$$\begin{aligned} R_{D^*} &\simeq R_{D^*}^{\text{SM}} \left(|1 + C_V^L|^2 + 0.05 |C_S^L|^2 + 16.27 |C_T^L|^2 \right. \\ &\quad - 0.13 \text{Re}[(1 + C_V^L)(C_S^L)^*] \\ &\quad - 5.0 \text{Re}[(1 + C_V^L)(C_T^L)^*] + 0.12 \text{Re}(C_{RL}^{\tau 3} + C_{LL}^{\tau 3}) \\ &\quad \left. + 0.05 |C_{RL}^{\tau 3} + C_{LL}^{\tau 3}|^2 \right), \end{aligned} \quad (26)$$

receive contributions from the \tilde{L} as well as from the H^\pm at the tree level. The Wilson coefficients corresponding to the \tilde{L} are given as [119]

$$\begin{aligned} C_V^L &= \frac{1}{2\sqrt{2}G_F m_{\tilde{L}}^2} \frac{\lambda_{23}^{\tilde{L}L} \lambda_{33}^{\tilde{L}L}}{2V_{cb}}, \\ C_S^L &= -\frac{1}{2\sqrt{2}G_F m_{\tilde{L}}^2} \frac{\lambda_{33}^{\tilde{L}L} \lambda_{23}^{\tilde{L}R}}{2V_{cb}}, \quad C_T^L = -\frac{1}{4} C_S^L, \end{aligned} \quad (27)$$

while those corresponding to the H^\pm are [98]

$$C_{RL}^{\tau 3} \approx \frac{m_b m_\tau}{m_{H^\pm}^2} \left(\frac{2}{t_\beta} + 1 \right), \quad C_{LL}^{\tau 3} = \frac{m_c m_\tau}{m_{H^\pm}^2} \quad (28)$$

(neglecting the highly subdominant $C_{LR}^{\tau 3}$ and $C_{RR}^{\tau 3}$ terms).

In our model, both the Q_1 and Q_2 should enter these Wilson coefficients, and their couplings relevant for this study thus include $\{\lambda_{23}^{Q_1 L}, \lambda_{32}^{Q_1 L}, \lambda_{33}^{Q_1 L}, \lambda_{23}^{Q_1 R}, \lambda_{32}^{Q_1 R}\}$ and $\{\lambda_{23}^{Q_2 L}, \lambda_{32}^{Q_2 L}, \lambda_{33}^{Q_2 L}, \lambda_{23}^{Q_2 R}, \lambda_{32}^{Q_2 R}\}$. Besides a_μ and $R_{D^{(*)}}$, combinations of these couplings are additionally constrained by the experimental results for

$$R_{K^{(*)}} \equiv \frac{\text{BR}(B \rightarrow K^{(*)} \mu^+ \mu^-)}{\text{BR}(B \rightarrow K^{(*)} e^+ e^-)} \propto \lambda_{23}^{\tilde{L}L*} \lambda_{33}^{\tilde{L}L} |\lambda_{32}^{\tilde{L}L}|^2, \quad (29)$$

and

$$R_K^\nu \equiv \frac{\text{BR}(B \rightarrow K \nu \nu)}{\text{BR}(B \rightarrow K \nu \nu)_{\text{SM}}} \propto \lambda_{23}^{\tilde{L}L*} \lambda_{33}^{\tilde{L}L}. \quad (30)$$

Furthermore, certain other observables, such as $\text{BR}(\tau \rightarrow \mu \gamma)$, $\text{BR}(\tau \rightarrow 3\mu)$, and $\text{BR}(B_c \rightarrow \tau \nu)$ also have a (slightly more involved) dependence on these couplings (see, e.g., [119] for their complete expressions).

IV. NUMERICAL ANALYSIS OF THE 2HDM+2 \tilde{L}

In order to verify that the values of Δa_μ and $R_{D^{(*)}}$ predicted by our model can be consistent with their experimental measurements given in Eqs. (2) and (3), respectively, we analyzed some representative low-energy configurations of its parameter space. We required these configurations to pass the following three criteria to be selected as benchmark points (BPs) for further analysis.

A. Yukawa RG running and perturbativity

All of our ten $\lambda^{Q_{1,2}}$ couplings, in addition to the t -quark Yukawa coupling, do not hit a Landau pole at high energies. For a parameter space point to qualify as a BP, these couplings should thus be small enough to stay in the perturbative realm up to the GUT scale. We ignore the rest of the SM Yukawa runnings, as they are considerably smaller. The 1-loop RG equations for the couplings of our concern are given in Appendix IV A. Also, as commonly done in literature, we run the RG equations from the EW scale all the way to the GUT scale, M_U , ignoring the effects of the intermediate symmetry-breaking scale, M_{PS} . These effects are also expected to be insignificant [122] since the running is logarithmic, and M_{PS} is quite close to the M_U in our model.

B. Direct search limits from the LHC

As discussed briefly in the previous section, the non-zero $\lambda_{23}^{\tilde{L}X}$, $\lambda_{32}^{\tilde{L}X}$, and $\lambda_{33}^{\tilde{L}L}$ couplings, with $X = L, R$, of each of the $\tilde{L}_{1,2}$ in our model would lead to some interesting signatures at the LHC, involving decay modes such as

$$\tilde{L} \rightarrow c\tau, \, s\nu, \, t\mu, \, b\nu, \, \text{and } \tau\tau,$$

where we have suppressed the neutrino flavours, as the LHC cannot mutually distinguish between them. Depending on the magnitudes of the couplings, the BRs in one or more of these modes can be sizeable. As a result, the pair-production of a given \tilde{L} at the LHC would give rise to different possibilities (third-generation quarks and leptons, third-generation quarks and second-generation leptons, etc.). Similarly, it would also have sizeable single-production, leading to more possible signatures. Some of these channels have been probed (see, e.g., Refs. [123–126]), while the prospects of some others at the high-luminosity LHC have also been studied [127–131]. The current direct-search exclusion bounds on a scalar leptoquark reach up to 1.7 TeV for maximal BR in some modes (see, e.g., Table 1 of Ref. [121]).

However, even such heavy leptoquarks can leave indirect signatures at the LHC, especially if they have large

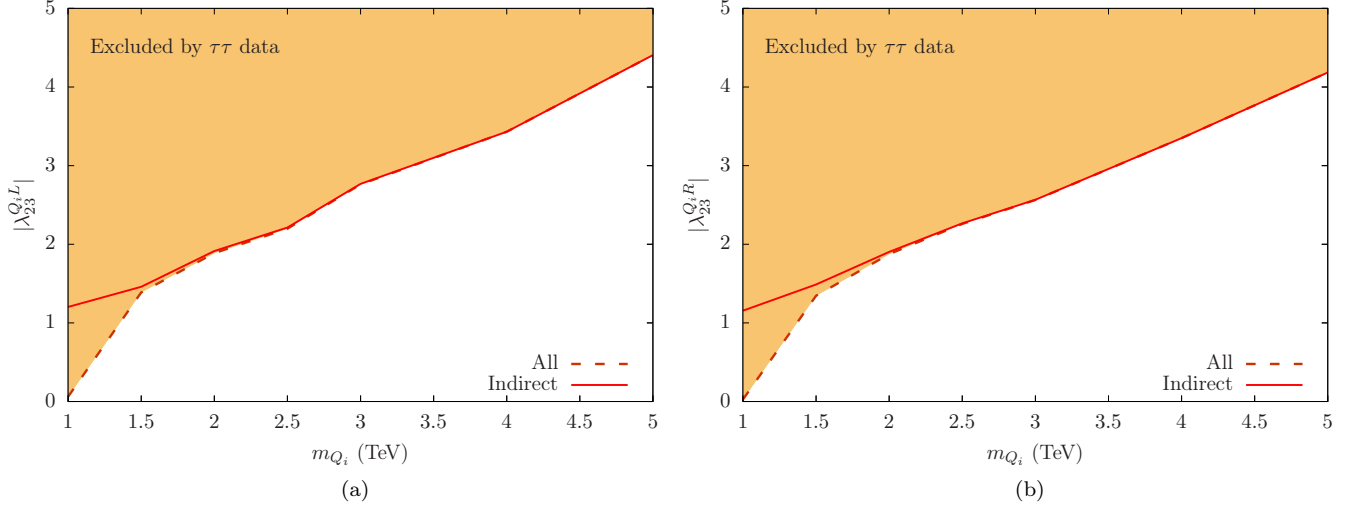


FIG. 2. Limits on Q_i couplings from ATLAS di- τ data [120] obtained following Refs. [49, 121]. The solid lines show the limits obtained by ignoring the contributions from the single- and pair-productions of the Q_i to the $\tau\tau$ data (the regions above the lines are excluded). The dashed lines show how the limits change if we do not neglect these processes but ignore the presence of all other couplings except the one under consideration.

Yukawa couplings. A pair of quarks can interchange a \tilde{L} in the t -channel and produce a lepton pair. As a result, with a large $\lambda_{23}^{\tilde{L}L}$ coupling, \tilde{L} could be responsible for a significant number of di-tau events at the LHC through the $c\bar{c} \rightarrow \tau^+\tau^-$ process. The process is highly sensitive to the unknown coupling, as the \tilde{L} -exchange diagram contributes to the cross section proportionally to the fourth power of $\lambda_{23}^{\tilde{L}L}$. Moreover, the \tilde{L} -mediated process and the SM $c\bar{c} \rightarrow Z^*/\gamma^* \rightarrow \tau^+\tau^-$ process undergo destructive interference, $\propto (\lambda_{23}^{\tilde{L}L})^2$. Overall, for $\lambda_{23}^{\tilde{L}L} \sim \mathcal{O}(1)$, the process would noticeably affect the $\tau\tau$ distributions. Hence, the current dilepton data can constrain the parameter space of a model [49, 121], as does the monolepton + missing transverse energy (MET) data for the \tilde{L} -mediated $qq' \rightarrow \ell\nu$ process. However, since Ref. [49] has shown the limits from the dilepton data to be stronger, we only consider these here. Moreover, the $\tau\tau jj$ direct-search bounds from the LHC [132, 133], recasted following the method described in Ref. [134], are similarly much weaker than the indirect bounds shown in Fig. 2.

Of the five non-zero couplings of each \tilde{L} in our analysis, the three $\lambda_{3i}^{\tilde{L}X}$ couplings are unaffected by the dilepton data. This is because a charge-1/3 \tilde{L} can couple to a charged lepton only with a t -quark through these couplings. Hence, one needs $t\bar{t}$ pairs in the initial state to produce $\mu^+\mu^-/\tau^+\tau^-$ pairs through \tilde{L} -exchange. But since the parton density function (PDF) of the t -quark is negligible, these couplings would not be constrained by the $\mu^+\mu^-$ or $\tau^+\tau^-$ (or even the μ/τ +MET) data. Finally, according to Ref. [134], search results for \tilde{L} pair-production in the $\ell t\ell t$ channels [135, 136] are also relatively much less constraining.

We show the exclusion limits on the absolute magnitudes of $\lambda_{23}^{\tilde{L}L}$ and $\lambda_{23}^{\tilde{L}R}$ from the ATLAS $\tau\tau$ data [120] in Figs. 2(a) and 2(b), respectively. (Recall that these two couplings contribute to the $R_{D^{(*)}}$ observables, but not to Δa_μ .) These limits are obtained by considering two degenerate LQs having $\lambda_{23}^{Q_1 L} = \lambda_{23}^{Q_2 L}$ (as is the case for our BPs 1, 3, and 5, described in the next section). Even though, we include the contributions from the single- and pair-production processes to the limits for completeness, these are relatively minor for the mass range we consider. For BPs 2 and 4, for which $\lambda_{23}^{Q_1 L} \neq \lambda_{23}^{Q_2 L}$, the coupling values are well within the allowed range. We have computed all the necessary cross-sections using the **Universal FeynRules Output (UFO)** [137] model files from Ref. [49] in MadGraph5 [138] with the NNPDF23LO [139] PDF set. We incorporated the QCD k -factor to compute the pair-production cross sections [140], and combined various production events following Refs. [141–143].

C. Indirect constraints

As noted in the previous section, a \tilde{L} can contribute to certain other flavor-changing decays, and its properties (i.e., mass and couplings) are therefore strongly constrained by the results of the experimental searches for these processes. A parameter space configuration was therefore acceptable only if it satisfied the constraints listed in Table II.

Observable	Range/limit
R_K	0.91 - 1.09
R_K^ν	< 2.7 [144]
$\text{BR}(\tau \rightarrow \mu\gamma)$	$< 4.4 \times 10^{-8}$
$\text{BR}(\tau \rightarrow 3\mu)$	$< 2.1 \times 10^{-8}$
$\text{BR}(B_c \rightarrow \tau\nu)$	< 0.1
$\text{BR}(B \rightarrow X_s\gamma)$	$\{3.17 - 3.47\} \times 10^{-4}$ [145]
$\text{BR}(B_s \rightarrow \mu\mu)$	$\{2.15 - 3.85\} \times 10^{-9}$ [146]
$\text{BR}(B_u \rightarrow \tau\nu)$	$\{0.87 - 1.25\} \times 10^{-4}$ [145]

TABLE II. Experimental constraints imposed on various observables in our analysis. For measurements, the 1σ statistical and systematic uncertainties, when given separately in the referenced result, were added in quadrature, while the upper limits quoted are at the 95% CL.

V. RESOLUTION OF FLAVOR ANOMALIES

In order to calculate the predictions of the various observables in the 2HDM+2 \tilde{L} , we incorporated it in the `Mathematica` package `SARAH-v4.14.4` [147–153]. This package automatically calculates the expressions for all the interaction vertices in order to write down model files for the `FORTRAN` code `SPheno-v4.0.5` [154, 155] for carrying out phenomenological studies. For a given input parameter space configuration, `SPheno` computes the mass spectra of all the particles in the model, as well as the decay BRs for some of them. It additionally computes the model predictions for most of the observables under consideration here, with the exception of $R_{D^{(*)}}$, R_K^ν , and $\text{BR}(B_c \rightarrow \tau\nu)$, which were estimated by implementing their expressions from [119] in a local numerical code.

The parameter values of the five BPs we analyse here are listed in Table III. Given that, despite fixing many of the model's parameters, the number of possible configurations of the 12 free ones meeting our requirements can potentially be very large (an exhaustive collection of which is beyond the scope of this study), we have identified these BPs using the following criteria.

- They satisfy all the constraints described in the previous section.
- The values of Δa_μ and $R_{D^{(*)}}$ lie almost exactly at the bottom of their respective $\pm 1\sigma$ ranges, given in Eqs. (2) and (3), i.e., $R_{D^*} \simeq 0.275$, and $\Delta a_\mu \simeq 20.1 \times 10^{-10}$.⁶ This means that the magnitude of any of the couplings for a given BP can not be reduced any further without adjusting some

other coupling to obtain the desired values of these observables.

- $m_{Q_1} = m_{Q_2}$, simply to reduce the number of free parameters to adjust. We will, however, briefly discuss the implications of a sizeable splitting between the masses of Q_1 and Q_2 later. Also, $m_{Q_{1,2}} \geq 2 \text{ TeV}$ ensures consistency with the strongest direct search bound noted in the previous section, irrespective of their mass-degeneracy and the sizes of their couplings.
- For BPs 1, 3, and 5, the corresponding couplings of Q_1 and Q_2 have exactly the same value. Furthermore, $\lambda_{23}^{Q_1 L} = -\lambda_{23}^{Q_2 R}$ (since consistency with the $R_{D^{(*)}}$ measurements warrants one of the relevant couplings to be negative), and $\lambda_{32}^{Q_1 L} = \lambda_{32}^{Q_2 R}$. These BPs thus represent the simplest possible scenario in the model, wherein the number of free parameters needed to meet all the enforced requirements is minimum. (We emphasize that none of these assumptions have been made on theoretical grounds.)
- BP2 is representative of an alternative possible scenario, in which Q_1 has couplings large enough to yield the minimum allowed values of Δa_μ and R_{D^*} , while the contribution of Q_2 is negligible. On the other hand, given the larger $m_{Q_{1,2}}$ for BP4, Q_2 contributes sizeably to R_{D^*} , since the couplings of Q_1 cannot get sufficiently large without violating perturbativity at the GUT scale. For both these points, again only for simplification, we set $\lambda_{23}^{Q_1 L} = -\lambda_{23}^{Q_2 R}$ and $\lambda_{32}^{Q_1 L} = \lambda_{32}^{Q_2 R}$.

The purpose of these BPs is to analyze the modifications needed in the various couplings for them to be consistent with the enforced constraints as the mass(es) of Q_1 or (and) Q_2 is (are) increased. The numerical values of each of the couplings given in the table are dictated by their perturbativity at the GUT scale, as well as the interplay between the experimental bounds on different observables. Thus, while $\lambda_{23}^{Q_{1,2} L}$ ($= -\lambda_{23}^{Q_{1,2} R}$) can all have substantially large magnitudes to satisfy $R_{D^{(*)}}$ for BPs 1 and 3 and still stay perturbative, $\lambda_{33}^{Q_{1,2} L}$ are restricted to much smaller values by the $R_K^\nu < 2.7$ limit. Similarly, $\lambda_{32}^{Q_1 L}$ can have values as large as 0.57 and 0.6, respectively, for BPs 2 and 4, but $\lambda_{32}^{Q_1 R}$ is strongly constrained by the upper limit on $\text{BR}(\tau \rightarrow \mu\gamma)$, as a result of which a slightly enhanced contribution is also needed from Q_2 to achieve $\Delta a_\mu \geq 20.1 \times 10^{-10}$ for these two BPs.

The RG running of the couplings is illustrated in Fig. 3 for BPs 1, 2, and 3 in the panels on the left, and for BPs 4 and 5 in the right column. In panels (b), (d) and (e), each of the 11 couplings is shown with a distinct line. In the remaining three panels, corresponding to BPs 1, 3, and 5, each line other than the one for y_t depicts the coupling pairs with identical magnitudes at the EW

⁶ The magnitudes of the couplings needed for R_{D^*} to reach the lower edge of its current experimental 1σ range are overall larger than for R_D . The former is therefore more constraining than the latter, and it is typically not possible to obtain the minimum allowed of values of both of these for a unique set of the relevant couplings.

	BP1	BP2	BP3	BP4	BP5
$m_{Q_{1,2}}$ (TeV)	2.0	2.0	2.5	2.5	3.0
$\lambda_{23}^{Q_1 L}$ $\lambda_{23}^{Q_2 L}$	0.53	0.71 0.01	0.66	0.78 0.42	0.8
$\lambda_{33}^{Q_1 L}$ $\lambda_{33}^{Q_2 L}$	0.032	0.1 0.01	0.038	0.12 0.015	0.046
$\lambda_{23}^{Q_1 R}$ $\lambda_{23}^{Q_2 R}$	-0.53	-0.71 -0.01	-0.66	-0.78 -0.42	-0.8
$\lambda_{32}^{Q_1 L}$ $\lambda_{32}^{Q_2 L}$	0.078	0.57 0.01	0.092	0.6 0.02	0.105
$\lambda_{32}^{Q_1 R}$ $\lambda_{32}^{Q_2 R}$	0.078	0.02 0.01	0.092	0.026 0.02	0.105
Γ_{Q_1} (GeV)	34.4	86.8	66.5	128	117
Γ_{Q_2} (GeV)		0.032		26.4	
BR($Q_1 \rightarrow s\nu_\tau$) BR($Q_2 \rightarrow s\nu_\tau$)	0.326	0.232 0.126	0.326	0.237 0.332	0.327
BR($Q_1 \rightarrow c\tau$) BR($Q_2 \rightarrow c\tau$)	0.636	0.453 0.255	0.637	0.464 0.648	0.638
BR($Q_1 \rightarrow b\nu_\mu$) BR($Q_2 \rightarrow b\nu_\mu$)	0.007	0.149 0.126	0.006	0.14 0.00	0.006
BR($Q_1 \rightarrow t\mu$) BR($Q_2 \rightarrow t\mu$)	0.014	0.147 0.247	0.012	0.139 0.00	0.011

TABLE III. Values of the input parameters, and of some Q_1 and Q_2 decay observables, for each of the five selected BPs.

scale, since the relevant RGEs, given in Appendix IV A, are symmetric under their interchange. BP1 has the most well-behaved running, as seen in Fig. 3(a), with all the couplings staying in the perturbative realm up to the GUT scale, which is to be expected, since their initial values are fairly small. The running is almost as good in Fig. 3(c), which actually represents a slightly modified BP2, wherein the mass and couplings of Q_1 are exactly as in Table III, but m_{Q_2} is set to 5 TeV. This modification is aimed at analysing whether an increase in the mass of Q_2 necessitates a large enough rise in the sizes of its couplings (which can be read off from Fig. 4(a)) to turn them non-perturbative. But since this BP was selected such that the couplings of Q_1 alone are sufficient for satisfying all the requirements, only a very small gradual enhancement in $\lambda_{32}^{Q_2 L} = \lambda_{32}^{Q_2 R}$ with rising m_{Q_2} is needed for obtaining the desired Δa_μ .

For BP3 (Fig. 3(e)) with $m_{Q_{1,2}} = 2.5$ TeV, some of the couplings, on account of being initially significantly larger than in BP1, start diverging near the GUT scale, but hit the Landau pole much later. As with BP2 above, the panels (d) and (e) correspond to BP4 with m_{Q_2} increased to 3 TeV and 3.5 TeV, respectively, while retaining the original values of the mass (2.5 TeV) and couplings of Q_1 . For $m_{Q_2} = 3$ TeV in panel (d), the divergence is much sharper for some of the couplings, compared to BP3, while for $M_{Q_2} = 3.5$ TeV in panel (e), most of the couplings hit the Landau pole just before M_U . Finally, due to the significantly larger initial values of some of the couplings in BP5, with $m_{Q_{1,2}} = 3$ TeV,

they turn non-perturbative way below the GUT scale, according to Fig. 3(f), thus invalidating our framework. Therefore, naively, we can conclude that i) $m_{Q_2} \simeq 3$ TeV is permissible in our model, as long as m_{Q_1} does not exceed 2.5 TeV, and ii) none of the $Q_{1,2}$ couplings can have a magnitude $\gtrsim 0.8$ at the EW scale for explaining the experimental data. The individual limits on $\lambda_{23}^{Q_{1,2} L}$ and $\lambda_{23}^{Q_{1,2} R}$ are very close to each other, as one would expect – the minor difference arises from the unequal couplings of the Z boson to the left- and right-handed fermions. It is, therefore, fair to assume that the limit on the combination $[(\lambda_{23}^{Q_{1,2} L})^2 + (\lambda_{23}^{Q_{1,2} R})^2]^{1/2}$ is also very similar.

Fig. 4(a) further illustrates the interplay between the theoretical and experimental constraints, as well as between the mass and couplings of Q_2 for BPs 2 and 4. For BP2, as pointed out previously, these couplings remain perturbative even for m_{Q_2} as large as 5 TeV (and hence more than twice the m_{Q_1}), while also fulfilling the conditions listed at the start of this section. In contrast, the large m_{Q_2} , and consequently the larger initial values of the (Q_1 and) Q_2 couplings needed to satisfy these conditions for BP4, drive the model into the non-perturbative realm for $m_{Q_2} \gtrsim 3$ TeV. Evidently, this interplay thus makes our model rather predictive, unlike many other competing (bottom-up) scenarios that have been investigated in the same context.

Fig. 4(b) shows some crucial differences in the LHC phenomenology of Q_2 between BPs 2 and 4. According to Table III, the very small Q_2 couplings in BP2 lead to its total width being four orders of magnitude smaller than that of Q_1 . Increasing the m_{Q_2} to 5 TeV for this BP has no visible impact on Γ_2 (notice that the corresponding green line for BP2 lies right on top of the bottom axis, and is almost invisible). On the other hand, $m_{Q_{1,2}} = 2.5$ TeV in BP4 already substantially increases the sizes of the couplings of Q_2 , and hence its total width, which further rises beyond 40 GeV for $m_{Q_2} \gtrsim 3$ TeV. Importantly though, $m_{Q_1} = m_{Q_2}$ for both these BPs would appear as a single resonance, with a width that is several tens of GeV, at the LHC. For a mass-splitting of $\mathcal{O}(100)$ GeV, on the other hand, it might be possible to individually resolve the peaks for Q_1 and Q_2 , which will be mutually well-separated.

Furthermore, both Q_1 and Q_2 for BP4 have the highest tree-level decay BR in the $c\tau$ mode, and the second highest one in the $s\nu_\tau$ channel, according to Fig. 4(b). Both these BRs remain almost constant for the entire range of m_{Q_2} (which is however much more strongly restricted by the perturbativity requirement compared to BP2, hence the shorter corresponding lines). For BP2, in contrast, the BRs of Q_2 in the $c\tau$ and $t\mu$ decay channels are almost equally dominant for $m_{Q_2} = 2$ TeV, but the latter immediately takes over and is by far the leading mode at $m_{Q_2} = 5$ TeV, where $b\nu_\mu$ is the next dominant channel. These unconventional search channels, despite the sub-GeV total width of Q_2 , may prove crucial for observing it simultaneously with the Q_1 at the LHC. The likelihood of its detection, when the $Q_{1,2}$ cou-

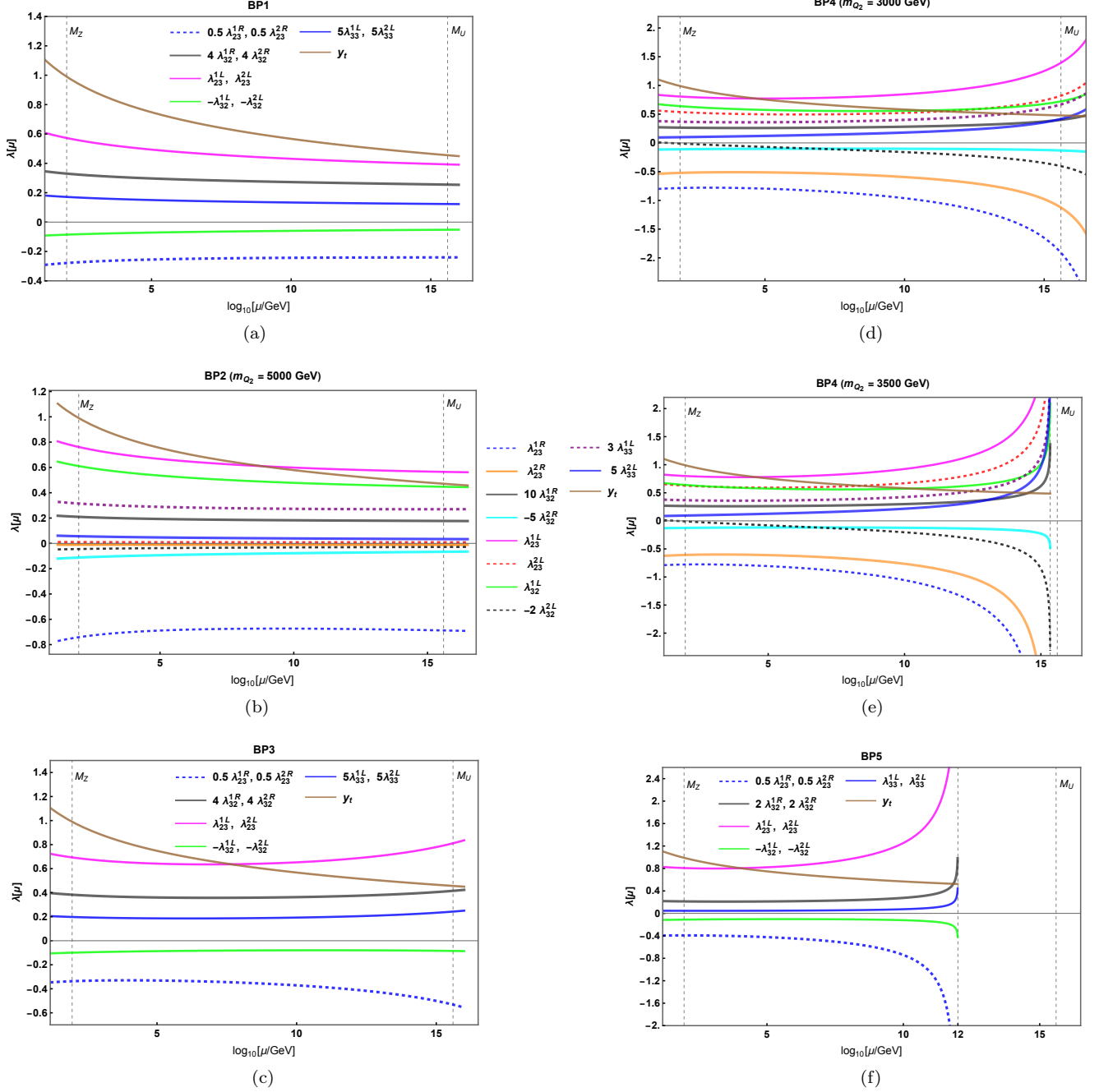


FIG. 3. The running of the leptoquark and t -Yukawa couplings for the 5 selected BPs. The panels (b), (d) and (e) share a common legend, whereas the legend for each of the other panels is shown within it. Some plots have been scaled for clarity.

plings are large enough to explain $R_{D^{(*)}}$ and Δa_μ both, but sufficiently small to remain perturbative at the GUT scale, should grow with $m_{Q_2} - m_{Q_1}$.

Finally, in Table V, we give approximate fermion mass values at the GUT scale for the original BPs 1 and 4, as well as for the modified BPs 2 and 4, along with their SM values at the same scale in the second column. The d -quark and e^- have the same mass in each of the two cases since they do not get contributions from the $Q_{1,2}$ couplings (see Eqs. (B16) and (B17)). These

GUT values of $m_{d,e}$ are, however, different from the SM in our model, since they run with the modified gauge couplings. The other mass values (and their ratios) change slightly (within $O(1)$) from those interpolated from the SM. Hence, we anticipate the results of the numerical fitting of our model's parameters to the SM data to be very similar to the ones obtained for the SO(10)-based models in a number of previous studies (see Refs. [61, 122, 156, 157] for recent examples). The purpose of this table is to provide an estimate of the

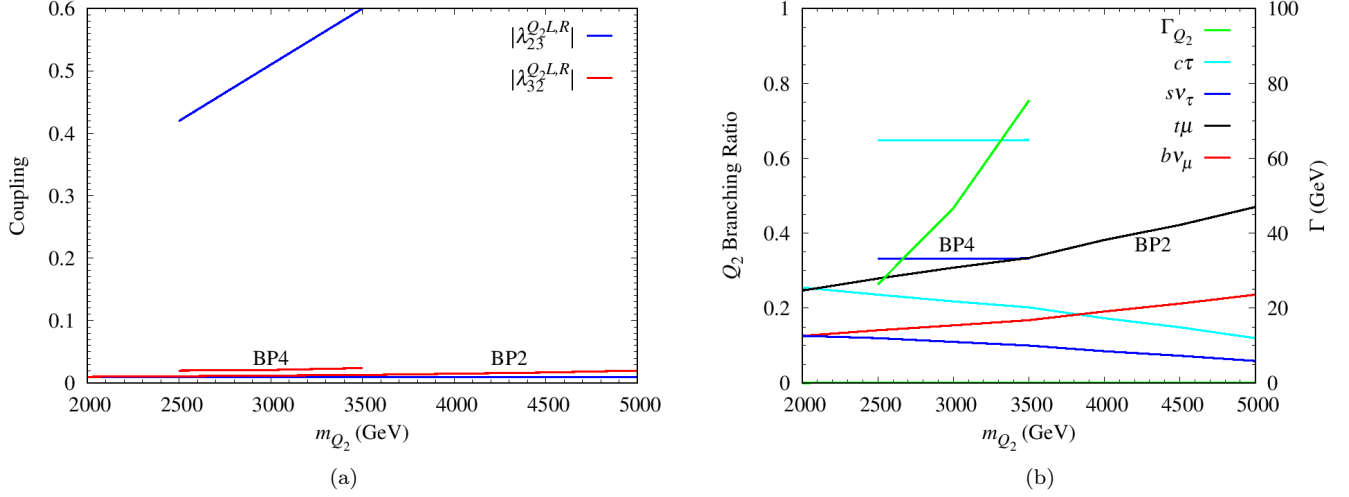


FIG. 4. Variation in (a) the Q_2 couplings needed to obtain the minimum acceptable values of $R_{D^{(*)}}$ and Δa_μ , and (b) its BRs with increasing mass, for BPs 2 (longer lines) and 4 (shorter lines).

deviation of the masses from the case when we have only the SM at the EW scale, while we leave the full numerical fitting for a future analysis.

VI. CONCLUSIONS

During recent years, many new physics candidates have been explored in order to explain the a_μ and $R_{D^{(*)}}$ anomalies that have persisted in the experimental data. One of the strongest candidates that has been claimed to resolve both these anomalies is a scalar leptoquark of the S_1 type. Most scenarios invoking such leptoquarks, or other plausible candidates, for this specific purpose, are nevertheless based on a bottom-up approach and do not attempt to offer a UV-complete picture consistent with many other questions pertinent in high energy physics.

In this article, we have taken the top-down approach of linking these anomalies to the SO(10) GUT group by proposing the existence of an entire complex $\mathbf{10}_H$ multiplet at the TeV scale, circumventing the well-known mass-splitting problem of GUT gauge groups. This multiplet contains two Higgs doublets and two S_1 -type leptoquarks – a combination very likely to address the mentioned collider anomalies. The Higgs sector of the resultant low-energy model resembles that of the Type-II 2HDM.

After discussing in detail the UV-complete framework as well as its low-energy limit – the Type-II 2HDM augmented with leptoquarks Q_1 and Q_2 – we have presented the results of our analysis of some sample configurations of the relevant parameters. This analysis aimed at testing the consistency of the model's predictions with not only the measurements of the a_μ and $R_{D^{(*)}}$ observables, but also several other important B -physics results as well as with the requirement of the perturbativity of

the couplings of interest. We have benchmarked two contrasting types of combinations of the Q_1 and Q_2 couplings, each of which is fairly small to remain perturbative up to the GUT scale without being in conflict with the direct and indirect search results for the S_1 -type leptoquark from the LHC.

ACKNOWLEDGEMENTS

We thank Arvind Bhaskar for helping us with the LHC bounds on leptoquark parameters. The work of UA was supported in part by the Chinese Academy of Sciences President's International Fellowship Initiative (PIFI) under Grant No. 2020PM0019; the Institute of High Energy Physics-Beijing, Chinese Academy of Sciences, under Contract No. Y9291220K (until June 2022); The Scientific and Technological Research Council of Türkiye (TÜBİTAK) BİDEB 2232-A program under project No. 121C067 (from September 2022). SMu would like to acknowledge support from the ICTP through the Associates Programme (2022-2023).

Appendix A: One-loop RG running of gauge couplings with a single intermediate scale

For a given particle content, the gauge couplings evolve under one-loop RG running in the $[M_A, M_B]$ energy interval as

$$\frac{1}{g_i^2(M_A)} - \frac{1}{g_i^2(M_B)} = \frac{a_i}{8\pi^2} \ln \frac{M_B}{M_A}, \quad (\text{A1})$$

where the RG coefficients a_i are given by [158, 159]

$$a_i = -\frac{11}{3}C_2(G_i) + \frac{2}{3} \sum_{R_f} T_i(R_f) \cdot d_1(R_f) \cdots d_n(R_f)$$

Fermion masses at M_U	SM	BP1	BP2 ($m_{Q_2} = 5$ TeV)	BP4	BP4 ($m_{Q_2} = 3$ TeV)
m_t/GeV	81.13	79.28	82.03	82.96	83.20
m_b/GeV	1.08	1.05	1.08	1.09	1.10
m_c/GeV	0.261	0.284	0.286	0.317	0.340
$m_s/(10^{-3}\text{GeV})$	23.35	18.40	18.36	19.21	19.7
$m_u/(10^{-3}\text{GeV})$	0.482	0.479	0.482	0.483	0.483
$m_d/(10^{-3}\text{GeV})$	1.229	0.929	0.929	0.929	0.929
m_τ/GeV	1.72	1.75	1.73	2.38	2.93
$m_\mu/(10^{-3}\text{GeV})$	101.3	78.7	84.4	86.5	87.1
$m_e/(10^{-3}\text{GeV})$	0.480	0.371	0.371	0.371	0.371

TABLE IV. Fermion masses at the unification scale $M_U = 10^{15.6}$ GeV for the original BPs 1 and 4, and for the modified BPs 2 and 4.

Representation	SU(2)	SU(3)	SU(4)
2	$\frac{1}{2}$	—	—
3	2	$\frac{1}{2}$	—
4	5	—	$\frac{1}{2}$
6	$\frac{35}{2}$	$\frac{5}{2}$	1
8	42	3	—
10	$\frac{165}{2}$	$\frac{15}{2}$	3
15	280	$10, \frac{35}{2}$	4

TABLE V. Dynkin indices T_i for various irreducible representations of the SU(2), SU(3), and SU(4) groups. Our normalization convention follows Ref. [159]. Notice that there are two inequivalent 15-dimensional irreducible representations for SU(3).

$$+ \frac{\eta}{3} \sum_{R_s} T_i(R_s) \cdot d_1(R_s) \cdots d_n(R_s). \quad (\text{A2})$$

The full gauge group is $G = G_i \otimes G_1 \otimes \dots \otimes G_n$. The summation in Eq. (A2) is over the irreducible representations of chiral fermions (R_f) and of scalars (R_s) in the second and third terms, respectively. The coefficient η is 1 for the complex representation, and 1/2 for the (pseudo-) real one. The symbol $d_j(R)$ denotes the dimension of the representation R under the group $G_{j \neq i}$. Finally, $C_2(G_i)$ represents the quadratic Casimir for the adjoint representation of the group G_i , whereas T_i is the Dynkin index of each representation (see Table A). Note that for the U(1) group, $C_2(G) = 0$, and

$$\sum_{f,s} T = \sum_{f,s} Y^2, \quad (\text{A3})$$

where Y is the $U(1)_Y$ charge.

The boundary/matching conditions at the symmetry-breaking scales for the sequence given in Eq. (9) are the

following.

$$\begin{aligned} M_U &: g_L(M_U) = g_R(M_U) = g_4(M_U), \\ M_{\text{PS}} &: g_3(M_{\text{PS}}) = g_4(M_{\text{PS}}), \quad g_2(M_{\text{PS}}) = g_L(M_{\text{PS}}), \\ &\quad \frac{1}{g_1^2(M_{\text{PS}})} = \frac{1}{g_R^2(M_{\text{PS}})} + \frac{2}{3} \frac{1}{g_4^2(M_{\text{PS}})}, \\ &\quad g_L(M_{\text{PS}}) = g_R(M_{\text{PS}}), \quad (\text{A4}) \\ M_Z &: \frac{1}{e^2(M_Z)} = \frac{1}{g_1^2(M_Z)} + \frac{1}{g_2^2(M_Z)}. \end{aligned}$$

Together with the matching and boundary conditions given in Eq. (A5), the one-loop RG running leads to the following conditions on the M_U and M_{PS} scales.

$$\begin{aligned} 2\pi \left[\frac{3 - 8 \sin^2 \theta_W(M_Z)}{\alpha(M_Z)} \right] &= (3a_1 - 5a_2) \ln \frac{M_{\text{PS}}}{M_Z} \\ &\quad + (-5a_L + 3a_R + 2a_4) \ln \frac{M_U}{M_{\text{PS}}}, \\ 2\pi \left[\frac{3}{\alpha(M_Z)} - \frac{8}{\alpha_s(M_Z)} \right] &= (3a_1 + 3a_2 - 8a_3) \ln \frac{M_{\text{PS}}}{M_Z} \\ &\quad + (3a_L + 3a_R - 6a_4) \ln \frac{M_U}{M_{\text{PS}}}, \quad (\text{A5}) \end{aligned}$$

where the notation of a_i is self-evident. The unified gauge coupling α_U at the scale M_U is then found as

$$\frac{2\pi}{\alpha_U} = \frac{2\pi}{\alpha_s(M_Z)} - \left(a_4 \ln \frac{M_U}{M_{\text{PS}}} + a_3 \ln \frac{M_{\text{PS}}}{M_Z} \right). \quad (\text{A6})$$

Appendix B: One-loop RG equations of the Yukawa couplings

The new Yukawa matrices in the Lagrangian given in Eq. (15) are defined in our setup as

$$\begin{aligned} \Lambda^{1L} &\rightarrow \begin{pmatrix} 0 & 0 & 0 \\ 0 & 0 & \lambda_{23}^{Q_1L} \\ 0 & \lambda_{32}^{Q_1L} & \lambda_{33}^{Q_1L} \end{pmatrix}, \quad \Lambda^{1R} \rightarrow \begin{pmatrix} 0 & 0 & 0 \\ 0 & 0 & \lambda_{23}^{Q_1R} \\ 0 & \lambda_{32}^{Q_1R} & 0 \end{pmatrix} \\ \Lambda^{2L} &\rightarrow \begin{pmatrix} 0 & 0 & 0 \\ 0 & 0 & \lambda_{23}^{Q_2L} \\ 0 & \lambda_{32}^{Q_2L} & \lambda_{33}^{Q_2L} \end{pmatrix}, \quad \Lambda^{2R} \rightarrow \begin{pmatrix} 0 & 0 & 0 \\ 0 & 0 & \lambda_{23}^{Q_2R} \\ 0 & \lambda_{32}^{Q_2R} & 0 \end{pmatrix}. \end{aligned}$$

The corresponding 1-loop RG equations, following Ref. [160] (or, alternatively, obtained by implementing the model in SARAH), are given below.

$$\begin{aligned}
16\pi^2\beta_{\lambda_{33}^{Q_2L}} &= 4\left(\lambda_{33}^{Q_2L}\right)^3 + \lambda_{33}^{Q_2L} \left[-\frac{5}{6}g_1^2 - \frac{9}{2}g_2^2 - 4g_3^2 \right. \\
&+ \frac{y_t^2}{2} + \frac{3}{2}\left(\lambda_{23}^{Q_1L}\right)^2 + \frac{1}{2}\left(\lambda_{32}^{Q_1L}\right)^2 + 4\left(\lambda_{33}^{Q_1L}\right)^2 \\
&+ 4\left(\lambda_{23}^{Q_2L}\right)^2 + 4\left(\lambda_{32}^{Q_2L}\right)^2 + \left(\lambda_{23}^{Q_2R}\right)^2 + \left(\lambda_{32}^{Q_2R}\right)^2 \Big] \\
&+ \lambda_{33}^{Q_1L} \left[\frac{5}{2}\lambda_{23}^{Q_1L}\lambda_{23}^{Q_2L} + \frac{7}{2}\lambda_{32}^{Q_1L}\lambda_{32}^{Q_2L} \right. \\
&+ \left. \lambda_{23}^{Q_1R}\lambda_{23}^{Q_2R} + \lambda_{32}^{Q_1R}\lambda_{32}^{Q_2R} \right] , \tag{B1}
\end{aligned}$$

$$\begin{aligned}
16\pi^2\beta_{\lambda_{32}^{Q_2L}} &= 4\left(\lambda_{32}^{Q_2L}\right)^3 + \lambda_{32}^{Q_2L} \left[-\frac{5}{6}g_1^2 - \frac{9}{2}g_2^2 - 4g_3^2 \right. \\
&+ \frac{y_t^2}{2} + 4\left(\lambda_{32}^{Q_1L}\right)^2 + \frac{1}{2}\left(\lambda_{33}^{Q_1L}\right)^2 + 2\left(\lambda_{23}^{Q_2L}\right)^2 \\
&+ 4\left(\lambda_{33}^{Q_2L}\right)^2 + \left(\lambda_{23}^{Q_2R}\right)^2 + \left(\lambda_{32}^{Q_2R}\right)^2 \Big] \\
&+ \lambda_{32}^{Q_1L} \left[2\lambda_{23}^{Q_1L}\lambda_{23}^{Q_2L} + \frac{7}{2}\lambda_{33}^{Q_1L}\lambda_{33}^{Q_2L} \right. \\
&+ \left. \lambda_{23}^{Q_1R}\lambda_{23}^{Q_2R} + \lambda_{32}^{Q_1R}\lambda_{32}^{Q_2R} \right] , \tag{B2}
\end{aligned}$$

$$\begin{aligned}
16\pi^2\beta_{\lambda_{23}^{Q_2L}} &= 4\left(\lambda_{23}^{Q_2L}\right)^3 + \lambda_{23}^{Q_2L} \left[-\frac{5}{6}g_1^2 - \frac{9}{2}g_2^2 - 4g_3^2 \right. \\
&+ 4\left(\lambda_{23}^{Q_1L}\right)^2 + \frac{3}{2}\left(\lambda_{33}^{Q_1L}\right)^2 + 2\left(\lambda_{32}^{Q_2L}\right)^2 \\
&+ 4\left(\lambda_{33}^{Q_2L}\right)^2 + \left(\lambda_{23}^{Q_2R}\right)^2 + \left(\lambda_{32}^{Q_2R}\right)^2 \Big] \\
&+ \lambda_{23}^{Q_1L} \left[2\lambda_{32}^{Q_1L}\lambda_{32}^{Q_2L} + \frac{5}{2}\lambda_{33}^{Q_1L}\lambda_{33}^{Q_2L} \right. \\
&+ \left. \lambda_{23}^{Q_1R}\lambda_{23}^{Q_2R} + \lambda_{32}^{Q_1R}\lambda_{32}^{Q_2R} \right] , \tag{B3}
\end{aligned}$$

$$\begin{aligned}
16\pi^2\beta_{\lambda_{33}^{Q_1L}} &= 4\left(\lambda_{33}^{Q_1L}\right)^3 + \lambda_{33}^{Q_1L} \left[-\frac{5}{6}g_1^2 - \frac{9}{2}g_2^2 - 4g_3^2 \right. \\
&+ \frac{y_t^2}{2} + 4\left(\lambda_{23}^{Q_1L}\right)^2 + 4\left(\lambda_{32}^{Q_1L}\right)^2 + \frac{3}{2}\left(\lambda_{23}^{Q_2L}\right)^2 \\
&+ \frac{1}{2}\left(\lambda_{32}^{Q_2L}\right)^2 + 4\left(\lambda_{33}^{Q_2L}\right)^2 + \left(\lambda_{23}^{Q_1R}\right)^2 + \left(\lambda_{32}^{Q_1R}\right)^2 \Big] \\
&+ \lambda_{33}^{Q_2L} \left[\frac{5}{2}\lambda_{23}^{Q_1L}\lambda_{23}^{Q_2L} + \frac{7}{2}\lambda_{32}^{Q_1L}\lambda_{32}^{Q_2L} \right. \\
&+ \left. \lambda_{23}^{Q_1R}\lambda_{23}^{Q_2R} + \lambda_{32}^{Q_1R}\lambda_{32}^{Q_2R} \right] , \tag{B4}
\end{aligned}$$

$$\begin{aligned}
16\pi^2\beta_{\lambda_{32}^{Q_1L}} &= 4\left(\lambda_{32}^{Q_1L}\right)^3 + \lambda_{32}^{Q_1L} \left[-\frac{5}{6}g_1^2 - \frac{9}{2}g_2^2 - 4g_3^2 \right. \\
&+ \frac{y_t^2}{2} + 4\left(\lambda_{33}^{Q_1L}\right)^2 + 2\left(\lambda_{23}^{Q_1L}\right)^2 + \left(\lambda_{23}^{Q_1R}\right)^2 \\
&+ \left(\lambda_{32}^{Q_1R}\right)^2 + 4\left(\lambda_{32}^{Q_2L}\right)^2 + \frac{1}{2}\left(\lambda_{33}^{Q_1L}\right)^2 \Big] \\
&+ \lambda_{32}^{Q_2L} \left[2\lambda_{23}^{Q_1L}\lambda_{23}^{Q_2L} + \frac{7}{2}\lambda_{33}^{Q_1L}\lambda_{33}^{Q_2L} \right. \\
&+ \left. \lambda_{23}^{Q_1R}\lambda_{23}^{Q_2R} + \lambda_{32}^{Q_1R}\lambda_{32}^{Q_2R} \right] , \tag{B5}
\end{aligned}$$

$$\begin{aligned}
16\pi^2\beta_{\lambda_{23}^{Q_1L}} &= 4\left(\lambda_{23}^{Q_1L}\right)^3 + \lambda_{23}^{Q_1L} \left[-\frac{5}{6}g_1^2 - \frac{9}{2}g_2^2 - 4g_3^2 \right. \\
&+ 2\left(\lambda_{32}^{Q_1L}\right)^2 + 4\left(\lambda_{33}^{Q_1L}\right)^2 + 4\left(\lambda_{23}^{Q_2L}\right)^2 \\
&+ \frac{3}{2}\left(\lambda_{33}^{Q_2L}\right)^2 + \left(\lambda_{23}^{Q_1R}\right)^2 + \left(\lambda_{32}^{Q_1R}\right)^2 \Big] \\
&+ \lambda_{23}^{Q_2L} \left[2\lambda_{32}^{Q_1L}\lambda_{32}^{Q_2L} + \frac{5}{2}\lambda_{33}^{Q_1L}\lambda_{33}^{Q_2L} \right. \\
&+ \left. \lambda_{23}^{Q_1R}\lambda_{23}^{Q_2R} + \lambda_{32}^{Q_1R}\lambda_{32}^{Q_2R} \right] , \tag{B6}
\end{aligned}$$

$$\begin{aligned}
16\pi^2\beta_{\lambda_{32}^{Q_2R}} &= 3\left(\lambda_{32}^{Q_2R}\right)^3 + \lambda_{32}^{Q_2R} \left[-\frac{13}{3}g_1^2 - 4g_3^2 + y_t^2 \right. \\
&+ 2\left(\lambda_{23}^{Q_2L}\right)^2 + 2\left(\lambda_{32}^{Q_2L}\right)^2 + 2\left(\lambda_{33}^{Q_2L}\right)^2 \Big] \\
&+ \left(\lambda_{23}^{Q_2R}\right)^2 + 3\left(\lambda_{32}^{Q_1R}\right)^2 + 2\lambda_{32}^{Q_1R} \left[\lambda_{23}^{Q_1L}\lambda_{23}^{Q_2L} \right. \\
&+ \left. \lambda_{32}^{Q_1L}\lambda_{32}^{Q_2L} + \lambda_{33}^{Q_1L}\lambda_{33}^{Q_2L} + \frac{1}{2}\lambda_{23}^{Q_1R}\lambda_{23}^{Q_2R} \right] , \tag{B7}
\end{aligned}$$

$$\begin{aligned}
16\pi^2\beta_{\lambda_{23}^{Q_2R}} &= 3\left(\lambda_{23}^{Q_2R}\right)^3 + \lambda_{23}^{Q_2R} \left[-\frac{13}{3}g_1^2 - 4g_3^2 \right. \\
&+ 2\left(\lambda_{23}^{Q_2L}\right)^2 + 2\left(\lambda_{32}^{Q_2L}\right)^2 + 2\left(\lambda_{33}^{Q_2L}\right)^2 + \left(\lambda_{32}^{Q_2R}\right)^2 \\
&+ 3\left(\lambda_{23}^{Q_1R}\right)^2 \Big] + 2\lambda_{23}^{Q_1R} \left[\lambda_{23}^{Q_1L}\lambda_{23}^{Q_2L} + \lambda_{32}^{Q_1L}\lambda_{32}^{Q_2L} \right. \\
&+ \left. \lambda_{33}^{Q_1L}\lambda_{33}^{Q_2L} + \frac{1}{2}\lambda_{32}^{Q_1R}\lambda_{32}^{Q_2R} \right] , \tag{B8}
\end{aligned}$$

$$\begin{aligned}
16\pi^2\beta_{\lambda_{32}^{Q_1R}} &= 3\left(\lambda_{32}^{Q_1R}\right)^3 + \lambda_{32}^{Q_1R} \left[-\frac{13}{3}g_1^2 - 4g_3^2 + y_t^2 \right. \\
&+ 2\left(\lambda_{23}^{Q_1L}\right)^2 + 2\left(\lambda_{32}^{Q_1L}\right)^2 + 2\left(\lambda_{33}^{Q_1L}\right)^2 + \left(\lambda_{23}^{Q_1R}\right)^2 \\
&+ 3\left(\lambda_{32}^{Q_2R}\right)^2 \Big] + 2\lambda_{32}^{Q_2R} \left[\lambda_{23}^{Q_1L}\lambda_{23}^{Q_2L} + \lambda_{32}^{Q_1L}\lambda_{32}^{Q_2L} \right. \\
&+ \left. \lambda_{33}^{Q_1L}\lambda_{33}^{Q_2L} + \frac{1}{2}\lambda_{23}^{Q_1R}\lambda_{23}^{Q_2R} \right] , \tag{B9}
\end{aligned}$$

$$\begin{aligned}
16\pi^2\beta_{\lambda_{23}^{Q_1R}} &= 3\left(\lambda_{23}^{Q_1R}\right)^3 + \lambda_{23}^{Q_1R}\left[-\frac{13}{3}g_1^2 - 4g_3^2\right. \\
&+ 2\left(\lambda_{23}^{Q_1L}\right)^2 + 2\left(\lambda_{32}^{Q_1L}\right)^2 + 2\left(\lambda_{33}^{Q_1L}\right)^2 + \left(\lambda_{32}^{Q_1R}\right)^2 \\
&+ 3\left(\lambda_{23}^{Q_2R}\right)^2\left. + 2\lambda_{23}^{Q_2R}\left[\lambda_{23}^{Q_1L}\lambda_{23}^{Q_2L} + \lambda_{32}^{Q_1L}\lambda_{32}^{Q_2L}\right.\right. \\
&\left. + \lambda_{33}^{Q_1L}\lambda_{33}^{Q_2L} + \frac{1}{2}\lambda_{32}^{Q_1R}\lambda_{32}^{Q_2R}\right]\left. \right], \quad (B10)
\end{aligned}$$

$$\begin{aligned}
16\pi^2\beta_{y_t} &= \frac{9}{2}y_t^3 + \frac{y_t}{2}\left[-\frac{17}{6}g_1^2 - \frac{9}{2}g_2^2 - 16g_3^2\right. \\
&+ \left(\lambda_{33}^{Q_1L}\right)^2 + \left(\lambda_{33}^{Q_2L}\right)^2 + \left(\lambda_{32}^{Q_1L}\right)^2 + \left(\lambda_{32}^{Q_2L}\right)^2 \\
&\left. + \left(\lambda_{32}^{Q_1R}\right)^2 + \left(\lambda_{32}^{Q_2R}\right)^2\right], \quad (B11)
\end{aligned}$$

$$\begin{aligned}
16\pi^2\beta_{y_c} &= \frac{y_c}{2}\left[6y_t^2 - \frac{17}{6}g_1^2 - \frac{9}{2}g_2^2 - 16g_3^2 + \left(\lambda_{23}^{Q_1L}\right)^2\right. \\
&\left. + \left(\lambda_{23}^{Q_2L}\right)^2 + \left(\lambda_{23}^{Q_1R}\right)^2 + \left(\lambda_{23}^{Q_2R}\right)^2\right], \quad (B12)
\end{aligned}$$

$$16\pi^2\beta_{y_u} = \frac{y_u}{2}\left[6y_t^2 - \frac{17}{6}g_1^2 - \frac{9}{2}g_2^2 - 16g_3^2\right], \quad (B13)$$

$$\begin{aligned}
16\pi^2\beta_{y_b} &= \frac{y_b}{2}\left[3y_t^2 - \frac{5}{6}g_1^2 - \frac{9}{2}g_2^2 - 16g_3^2 + \left(\lambda_{32}^{Q_1L}\right)^2\right. \\
&\left. + \left(\lambda_{32}^{Q_2L}\right)^2 + \left(\lambda_{33}^{Q_1L}\right)^2 + \left(\lambda_{33}^{Q_2L}\right)^2\right], \quad (B14)
\end{aligned}$$

$$\begin{aligned}
16\pi^2\beta_{y_s} &= \frac{y_s}{2}\left[-\frac{5}{6}g_1^2 - \frac{9}{2}g_2^2 - 16g_3^2\right. \\
&\left. + \left(\lambda_{23}^{Q_1L}\right)^2 + \left(\lambda_{23}^{Q_2L}\right)^2\right], \quad (B15)
\end{aligned}$$

$$16\pi^2\beta_{y_d} = \frac{y_d}{2}\left[-\frac{5}{6}g_1^2 - \frac{9}{2}g_2^2 - 16g_3^2\right], \quad (B16)$$

$$16\pi^2\beta_{y_e} = \frac{y_e}{2}\left[-\frac{15}{2}g_1^2 - \frac{9}{2}g_2^2\right], \quad (B17)$$

$$\begin{aligned}
16\pi^2\beta_{y_\tau} &= \frac{3y_\tau}{2}\left[-\frac{5}{2}g_1^2 - \frac{3}{2}g_2^2 + \left(\lambda_{23}^{Q_1L}\right)^2\right. \\
&+ \left(\lambda_{23}^{Q_2L}\right)^2 + \left(\lambda_{33}^{Q_1L}\right)^2 + \left(\lambda_{33}^{Q_2L}\right)^2 \\
&\left. + \left(\lambda_{23}^{Q_1R}\right)^2 + \left(\lambda_{23}^{Q_2R}\right)^2\right], \quad (B18)
\end{aligned}$$

$$\begin{aligned}
16\pi^2\beta_{y_\mu} &= \frac{3y_\mu}{2}\left[-\frac{5}{2}g_1^2 - \frac{3}{2}g_2^2 + \left(\lambda_{32}^{Q_1L}\right)^2\right. \\
&\left. + \left(\lambda_{32}^{Q_2L}\right)^2 + \left(\lambda_{32}^{Q_1R}\right)^2 + \left(\lambda_{32}^{Q_2R}\right)^2\right]. \quad (B19)
\end{aligned}$$

-
- [1] J. P. Lees *et al.* (BaBar Collaboration), “Evidence for an excess of $\bar{B} \rightarrow D^{(*)}\tau^-\bar{\nu}_\tau$ decays,” *Phys. Rev. Lett.* **109**, 101802 (2012), [arXiv:1205.5442 \[hep-ex\]](#).
- [2] J. P. Lees *et al.* (BaBar Collaboration), “Measurement of an Excess of $\bar{B} \rightarrow D^{(*)}\tau^-\bar{\nu}_\tau$ Decays and Implications for Charged Higgs Bosons,” *Phys. Rev. D* **88**, 072012 (2013), [arXiv:1303.0571 \[hep-ex\]](#).
- [3] Roel Aaij *et al.* (LHCb Collaboration), “Test of lepton universality using $B^+ \rightarrow K^+\ell^+\ell^-$ decays,” *Phys. Rev. Lett.* **113**, 151601 (2014), [arXiv:1406.6482 \[hep-ex\]](#).
- [4] R. Aaij *et al.* (LHCb Collaboration), “Test of lepton universality with $B^0 \rightarrow K^{*0}\ell^+\ell^-$ decays,” *JHEP* **08**, 055 (2017), [arXiv:1705.05802 \[hep-ex\]](#).
- [5] Roel Aaij *et al.* (LHCb Collaboration), “Measurement of the ratio of branching fractions $\mathcal{B}(\bar{B}^0 \rightarrow D^{*+}\tau^-\bar{\nu}_\tau)/\mathcal{B}(\bar{B}^0 \rightarrow D^{*+}\mu^-\bar{\nu}_\mu)$,” *Phys. Rev. Lett.* **115**, 111803 (2015), [Erratum: *Phys. Rev. Lett.* **115**, 159901 (2015)], [arXiv:1506.08614 \[hep-ex\]](#).
- [6] R. Aaij *et al.* (LHCb Collaboration), “Measurement of the ratio of the $B^0 \rightarrow D^{*+}\tau^+\nu_\tau$ and $B^0 \rightarrow D^{*+}\mu^+\nu_\mu$ branching fractions using three-prong τ -lepton decays,” *Phys. Rev. Lett.* **120**, 171802 (2018), [arXiv:1708.08856 \[hep-ex\]](#).
- [7] R. Aaij *et al.* (LHCb Collaboration), “Test of Lepton Flavor Universality by the measurement of the $B^0 \rightarrow D^{*+}\tau^+\nu_\tau$ branching fraction using three-prong τ decays,” *Phys. Rev. D* **97**, 072013 (2018), [arXiv:1711.02505 \[hep-ex\]](#).
- [8] S. Hirose *et al.* (Belle Collaboration), “Measurement of the τ lepton polarization and $R(D^*)$ in the decay $\bar{B} \rightarrow D^{*+}\tau^-\bar{\nu}_\tau$,” *Phys. Rev. Lett.* **118**, 211801 (2017), [arXiv:1612.00529 \[hep-ex\]](#).
- [9] S. Hirose *et al.* (Belle Collaboration), “Measurement of the τ lepton polarization and $R(D^*)$ in the decay $\bar{B} \rightarrow D^{*+}\tau^-\bar{\nu}_\tau$ with one-prong hadronic τ decays at Belle,” *Phys. Rev. D* **97**, 012004 (2018), [arXiv:1709.00129 \[hep-ex\]](#).
- [10] <https://hflav-eos.web.cern.ch/hflav-eos/semi/moriond24/html/RDsDsstar/RDRDs>.
- [11] Yasmine Sara Amhis *et al.* (HFLAV Collaboration), “Averages of b-hadron, c-hadron, and τ -lepton properties as of 2021,” *Phys. Rev. D* **107**, 052008 (2023), [arXiv:2206.07501 \[hep-ex\]](#).
- [12] G. W. Bennett *et al.* (Muon g-2 Collaboration), “Final

- Report of the Muon E821 Anomalous Magnetic Moment Measurement at BNL,” *Phys. Rev. D* **73**, 072003 (2006), [arXiv:hep-ex/0602035](#).
- [13] D. P. Aguillard *et al.* (Muon g-2 Collaboration), “Measurement of the Positive Muon Anomalous Magnetic Moment to 0.20 ppm,” *Phys. Rev. Lett.* **131**, 161802 (2023), [arXiv:2308.06230 \[hep-ex\]](#).
- [14] Andrzej Czarnecki, William J. Marciano, and Arkady Vainshtein, “Refinements in electroweak contributions to the muon anomalous magnetic moment,” *Phys. Rev. D* **67**, 073006 (2003), [Erratum: *Phys. Rev. D* **73**, 119901 (2006)], [arXiv:hep-ph/0212229](#).
- [15] Kirill Melnikov and Arkady Vainshtein, “Hadronic light-by-light scattering contribution to the muon anomalous magnetic moment revisited,” *Phys. Rev. D* **70**, 113006 (2004), [arXiv:hep-ph/0312226](#).
- [16] Tatsumi Aoyama, Masashi Hayakawa, Toichiro Kinoshita, and Makiko Nio, “Complete Tenth-Order QED Contribution to the Muon g-2,” *Phys. Rev. Lett.* **109**, 111808 (2012), [arXiv:1205.5370 \[hep-ph\]](#).
- [17] C. Gnendiger, D. Stöckinger, and H. Stöckinger-Kim, “The electroweak contributions to $(g - 2)_\mu$ after the Higgs boson mass measurement,” *Phys. Rev. D* **88**, 053005 (2013), [arXiv:1306.5546 \[hep-ph\]](#).
- [18] Alexander Kurz, Tao Liu, Peter Marquard, and Matthias Steinhauser, “Hadronic contribution to the muon anomalous magnetic moment to next-to-next-to-leading order,” *Phys. Lett. B* **734**, 144–147 (2014), [arXiv:1403.6400 \[hep-ph\]](#).
- [19] Gilberto Colangelo, Martin Hoferichter, Andreas Nyffeler, Massimo Passera, and Peter Stoffer, “Remarks on higher-order hadronic corrections to the muon g-2,” *Phys. Lett. B* **735**, 90–91 (2014), [arXiv:1403.7512 \[hep-ph\]](#).
- [20] Gilberto Colangelo, Martin Hoferichter, Massimiliano Procura, and Peter Stoffer, “Dispersion relation for hadronic light-by-light scattering: two-pion contributions,” *JHEP* **04**, 161 (2017), [arXiv:1702.07347 \[hep-ph\]](#).
- [21] Michel Davier, Andreas Hoecker, Bogdan Malaescu, and Zhiqing Zhang, “Reevaluation of the hadronic vacuum polarisation contributions to the Standard Model predictions of the muon $g - 2$ and $\alpha(m_Z^2)$ using newest hadronic cross-section data,” *Eur. Phys. J. C* **77**, 827 (2017), [arXiv:1706.09436 \[hep-ph\]](#).
- [22] Pere Masjuan and Pablo Sanchez-Puertas, “Pseudoscalar-pole contribution to the $(g_\mu - 2)$: a rational approach,” *Phys. Rev. D* **95**, 054026 (2017), [arXiv:1701.05829 \[hep-ph\]](#).
- [23] Alexander Keshavarzi, Daisuke Nomura, and Thomas Teubner, “Muon $g - 2$ and $\alpha(m_Z^2)$: a new data-based analysis,” *Phys. Rev. D* **97**, 114025 (2018), [arXiv:1802.02995 \[hep-ph\]](#).
- [24] Martin Hoferichter, Bai-Long Hoid, Bastian Kubis, Stefan Leupold, and Sebastian P. Schneider, “Dispersion relation for hadronic light-by-light scattering: pion pole,” *JHEP* **10**, 141 (2018), [arXiv:1808.04823 \[hep-ph\]](#).
- [25] Gilberto Colangelo, Martin Hoferichter, and Peter Stoffer, “Two-pion contribution to hadronic vacuum polarization,” *JHEP* **02**, 006 (2019), [arXiv:1810.00007 \[hep-ph\]](#).
- [26] Antoine Gérardin, Harvey B. Meyer, and Andreas Nyffeler, “Lattice calculation of the pion transition form factor with $N_f = 2+1$ Wilson quarks,” *Phys. Rev. D* **100**, 034520 (2019), [arXiv:1903.09471 \[hep-lat\]](#).
- [27] Martin Hoferichter, Bai-Long Hoid, and Bastian Kubis, “Three-pion contribution to hadronic vacuum polarization,” *JHEP* **08**, 137 (2019), [arXiv:1907.01556 \[hep-ph\]](#).
- [28] M. Davier, A. Hoecker, B. Malaescu, and Z. Zhang, “A new evaluation of the hadronic vacuum polarisation contributions to the muon anomalous magnetic moment and to $\alpha(m_Z^2)$,” *Eur. Phys. J. C* **80**, 241 (2020), [Erratum: *Eur. Phys. J. C* **80**, 410 (2020)], [arXiv:1908.00921 \[hep-ph\]](#).
- [29] Johan Bijnens, Nils Hermansson-Truedsson, and Antonio Rodríguez-Sánchez, “Short-distance constraints for the HLbL contribution to the muon anomalous magnetic moment,” *Phys. Lett. B* **798**, 134994 (2019), [arXiv:1908.03331 \[hep-ph\]](#).
- [30] Gilberto Colangelo, Franziska Hagelstein, Martin Hoferichter, Laetitia Laub, and Peter Stoffer, “Longitudinal short-distance constraints for the hadronic light-by-light contribution to $(g - 2)_\mu$ with large- N_c Regge models,” *JHEP* **03**, 101 (2020), [arXiv:1910.13432 \[hep-ph\]](#).
- [31] Thomas Blum, Norman Christ, Masashi Hayakawa, Taku Izubuchi, Luchang Jin, Chulwoo Jung, and Christoph Lehner, “Hadronic Light-by-Light Scattering Contribution to the Muon Anomalous Magnetic Moment from Lattice QCD,” *Phys. Rev. Lett.* **124**, 132002 (2020), [arXiv:1911.08123 \[hep-lat\]](#).
- [32] Alexander Keshavarzi, Daisuke Nomura, and Thomas Teubner, “ $g - 2$ of charged leptons, $\alpha(M_Z^2)$, and the hyperfine splitting of muonium,” *Phys. Rev. D* **101**, 014029 (2020), [arXiv:1911.00367 \[hep-ph\]](#).
- [33] Tatsumi Aoyama, Toichiro Kinoshita, and Makiko Nio, “Theory of the Anomalous Magnetic Moment of the Electron,” *Atoms* **7**, 28 (2019).
- [34] T. Aoyama *et al.*, “The anomalous magnetic moment of the muon in the Standard Model,” *Phys. Rept.* **887**, 1–166 (2020), [arXiv:2006.04822 \[hep-ph\]](#).
- [35] Yasuhito Sakaki, Minoru Tanaka, Andrey Tayduganov, and Ryoutaro Watanabe, “Testing leptoquark models in $\bar{B} \rightarrow D^{(*)}\tau\bar{\nu}$,” *Phys. Rev. D* **88**, 094012 (2013), [arXiv:1309.0301 \[hep-ph\]](#).
- [36] Béranger Dumont, Kenji Nishiwaki, and Ryoutaro Watanabe, “LHC constraints and prospects for S_1 scalar leptoquark explaining the $\bar{B} \rightarrow D^{(*)}\tau\bar{\nu}$ anomaly,” *Phys. Rev. D* **94**, 034001 (2016), [arXiv:1603.05248 \[hep-ph\]](#).
- [37] Marat Freytsis, Zoltan Ligeti, and Joshua T. Ruderman, “Flavor models for $\bar{B} \rightarrow D^{(*)}\tau\bar{\nu}$,” *Phys. Rev. D* **92**, 054018 (2015), [arXiv:1506.08896 \[hep-ph\]](#).
- [38] Martin Bauer and Matthias Neubert, “Minimal Leptoquark Explanation for the $R_{D^{(*)}}$, R_K , and $(g - 2)_\mu$ Anomalies,” *Phys. Rev. Lett.* **116**, 141802 (2016), [arXiv:1511.01900 \[hep-ph\]](#).
- [39] Diganta Das, Chandan Hati, Girish Kumar, and Namit Mahajan, “Towards a unified explanation of $R_{D^{(*)}}$, R_K and $(g - 2)_\mu$ anomalies in a left-right model with leptoquarks,” *Phys. Rev. D* **94**, 055034 (2016), [arXiv:1605.06313 \[hep-ph\]](#).
- [40] Gudrun Hiller, Dennis Loose, and Kay Schönwald, “Leptoquark Flavor Patterns & B Decay Anomalies,”

- JHEP **12**, 027 (2016), [arXiv:1609.08895 \[hep-ph\]](#).
- [41] Estefania Coluccio Leskow, Giancarlo D’Ambrosio, Andreas Crivellin, and Dario Müller, “ $(g - 2)_\mu$, lepton flavor violation, and Z decays with leptoquarks: Correlations and future prospects,” *Phys. Rev. D* **95**, 055018 (2017), [arXiv:1612.06858 \[hep-ph\]](#).
 - [42] Andreas Crivellin, Dario Müller, and Toshihiko Ota, “Simultaneous explanation of $R(D^{(*)})$ and $b \rightarrow s\mu^+\mu^-$: the last scalar leptoquarks standing,” *JHEP* **09**, 040 (2017), [arXiv:1703.09226 \[hep-ph\]](#).
 - [43] Yi Cai, John Gargalionis, Michael A. Schmidt, and Raymond R. Volkas, “Reconsidering the One Leptoquark solution: flavor anomalies and neutrino mass,” *JHEP* **10**, 047 (2017), [arXiv:1704.05849 \[hep-ph\]](#).
 - [44] David Marzocca, “Addressing the B-physics anomalies in a fundamental Composite Higgs Model,” *JHEP* **07**, 121 (2018), [arXiv:1803.10972 \[hep-ph\]](#).
 - [45] Ufuk Aydemir, Djordje Minic, Chen Sun, and Tatsuo Takeuchi, “ B -decay anomalies and scalar leptoquarks in unified Pati-Salam models from noncommutative geometry,” *JHEP* **09**, 117 (2018), [arXiv:1804.05844 \[hep-ph\]](#).
 - [46] Damir Bečirević, Ilja Doršner, Svjetlana Fajfer, Nejc Košnik, Darius A. Faroughy, and Olcyr Sumensari, “Scalar leptoquarks from grand unified theories to accommodate the B -physics anomalies,” *Phys. Rev. D* **98**, 055003 (2018), [arXiv:1806.05689 \[hep-ph\]](#).
 - [47] A. Angelescu, Damir Bečirević, D. A. Faroughy, and O. Sumensari, “Closing the window on single leptoquark solutions to the B -physics anomalies,” *JHEP* **10**, 183 (2018), [arXiv:1808.08179 \[hep-ph\]](#).
 - [48] Julian Heeck and Daniele Teresi, “Pati-Salam explanations of the B-meson anomalies,” *JHEP* **12**, 103 (2018), [arXiv:1808.07492 \[hep-ph\]](#).
 - [49] Tanumoy Mandal, Subhadip Mitra, and Swapnil Raz, “ $R_{D^{(*)}}$ motivated S_1 leptoquark scenarios: Impact of interference on the exclusion limits from LHC data,” *Phys. Rev. D* **99**, 055028 (2019), [arXiv:1811.03561 \[hep-ph\]](#).
 - [50] Ufuk Aydemir, Tanumoy Mandal, and Subhadip Mitra, “Addressing the $R_{D^{(*)}}$ anomalies with an S_1 leptoquark from $SO(10)$ grand unification,” *Phys. Rev. D* **101**, 015011 (2020), [arXiv:1902.08108 \[hep-ph\]](#).
 - [51] Andreas Crivellin, Dario Müller, and Francesco Saturnino, “Flavor Phenomenology of the Leptoquark Singlet-Triplet Model,” *JHEP* **06**, 020 (2020), [arXiv:1912.04224 \[hep-ph\]](#).
 - [52] David Marzocca and Sokratis Trifinopoulos, “Minimal Explanation of Flavor Anomalies: B-Meson Decays, Muon Magnetic Moment, and the Cabibbo Angle,” *Phys. Rev. Lett.* **127**, 061803 (2021), [arXiv:2104.05730 \[hep-ph\]](#).
 - [53] Arvind Bhaskar, Anirudhan A. Madathil, Tanumoy Mandal, and Subhadip Mitra, “Combined explanation of W -mass, muon $g - 2$, $R_{K^{(*)}}$ and $R_{D^{(*)}}$ anomalies in a singlet-triplet scalar leptoquark model,” *Phys. Rev. D* **106**, 115009 (2022), [arXiv:2204.09031 \[hep-ph\]](#).
 - [54] Arvind Bhaskar, Diganta Das, Soumyadip Kundu, Anirudhan A. Madathil, Tanumoy Mandal, and Subhadip Mitra, “Vector leptoquark contributions to lepton dipole moments,” (2024), [arXiv:2408.11798 \[hep-ph\]](#).
 - [55] Roel Aaij *et al.* (LHCb Collaboration), “Search for lepton-universality violation in $B^+ \rightarrow K^+\ell^+\ell^-$ decays,” *Phys. Rev. Lett.* **122**, 191801 (2019), [arXiv:1903.09252 \[hep-ex\]](#).
 - [56] “Test of lepton universality in $b \rightarrow s\ell^+\ell^-$ decays,” (2022), [arXiv:2212.09152 \[hep-ex\]](#).
 - [57] Borut Bajc, Alejandra Melfo, Goran Senjanovic, and Francesco Vissani, “Yukawa sector in non-supersymmetric renormalizable $SO(10)$,” *Phys. Rev. D* **73**, 055001 (2006), [arXiv:hep-ph/0510139 \[hep-ph\]](#).
 - [58] K. S. Babu and S. Khan, “Minimal nonsupersymmetric $SO(10)$ model: Gauge coupling unification, proton decay, and fermion masses,” *Phys. Rev. D* **92**, 075018 (2015), [arXiv:1507.06712 \[hep-ph\]](#).
 - [59] K. S. Babu, Borut Bajc, and Shaikh Saad, “Yukawa Sector of Minimal $SO(10)$ Unification,” *JHEP* **02**, 136 (2017), [arXiv:1612.04329 \[hep-ph\]](#).
 - [60] G.C. Branco, P.M. Ferreira, L. Lavoura, M.N. Rebelo, Marc Sher, *et al.*, “Theory and phenomenology of two-Higgs-doublet models,” *Phys. Rept.* **516**, 1–102 (2012), [arXiv:1106.0034 \[hep-ph\]](#).
 - [61] Guido Altarelli and Davide Meloni, “A non supersymmetric $SO(10)$ grand unified model for all the physics below M_{GUT} ,” *JHEP* **08**, 021 (2013), [arXiv:1305.1001 \[hep-ph\]](#).
 - [62] R. D. Peccei and Helen R. Quinn, “CP Conservation in the Presence of Instantons,” *Phys. Rev. Lett.* **38**, 1440–1443 (1977).
 - [63] Steven Weinberg, “A New Light Boson?” *Phys. Rev. Lett.* **40**, 223–226 (1978).
 - [64] Frank Wilczek, “Problem of Strong P and T Invariance in the Presence of Instantons,” *Phys. Rev. Lett.* **40**, 279–282 (1978).
 - [65] K. S. Babu and R. N. Mohapatra, “Predictive neutrino spectrum in minimal $SO(10)$ grand unification,” *Phys. Rev. Lett.* **70**, 2845–2848 (1993), [arXiv:hep-ph/9209215](#).
 - [66] Anne Ernst, Andreas Ringwald, and Carlos Tamarit, “Axion Predictions in $SO(10) \times U(1)_{PQ}$ Models,” *JHEP* **02**, 103 (2018), [arXiv:1801.04906 \[hep-ph\]](#).
 - [67] Alessandro Broggio, Eung Jin Chun, Massimo Passera, Ketan M. Patel, and Sudhir K. Vempati, “Limiting two-Higgs-doublet models,” *JHEP* **11**, 058 (2014), [arXiv:1409.3199 \[hep-ph\]](#).
 - [68] Lei Wang and Xiao-Fang Han, “A light pseudoscalar of 2HDM confronted with muon $g-2$ and experimental constraints,” *JHEP* **05**, 039 (2015), [arXiv:1412.4874 \[hep-ph\]](#).
 - [69] Victor Ilisie, “New Barr-Zee contributions to $(g - 2)_\mu$ in two-Higgs-doublet models,” *JHEP* **04**, 077 (2015), [arXiv:1502.04199 \[hep-ph\]](#).
 - [70] Yuji Omura, Eibun Senaha, and Kazuhiro Tobe, “Lepton-flavor-violating Higgs decay $h \rightarrow \mu\tau$ and muon anomalous magnetic moment in a general two Higgs doublet model,” *JHEP* **05**, 028 (2015), [arXiv:1502.07824 \[hep-ph\]](#).
 - [71] Tomohiro Abe, Ryosuke Sato, and Kei Yagyu, “Lepton-specific two Higgs doublet model as a solution of muon $g - 2$ anomaly,” *JHEP* **07**, 064 (2015), [arXiv:1504.07059 \[hep-ph\]](#).
 - [72] Eung Jin Chun, Zhaofeng Kang, Michihisa Takeuchi, and Yue-Lin Sming Tsai, “LHC τ -rich tests of lepton-specific 2HDM for $(g - 2)_\mu$,” *JHEP* **11**, 099 (2015), [arXiv:1507.08067 \[hep-ph\]](#).

- [73] Eung Jin Chun, “The muon $g - 2$ in two-Higgs-doublet models,” *EPJ Web Conf.* **118**, 01006 (2016), [arXiv:1511.05225 \[hep-ph\]](#).
- [74] Tao Han, Sin Kyu Kang, and Joshua Sayre, “Muon $g - 2$ in the aligned two Higgs doublet model,” *JHEP* **02**, 097 (2016), [arXiv:1511.05162 \[hep-ph\]](#).
- [75] Eung Jin Chun and Jinsu Kim, “Leptonic Precision Test of Leptophilic Two-Higgs-Doublet Model,” *JHEP* **07**, 110 (2016), [arXiv:1605.06298 \[hep-ph\]](#).
- [76] Adriano Cherkiglia, Patrick Kneschke, Dominik Stöckinger, and Hyejung Stöckinger-Kim, “The muon magnetic moment in the 2HDM: complete two-loop result,” *JHEP* **01**, 007 (2017), [Erratum: *JHEP* **10**, 242 (2021)], [arXiv:1607.06292 \[hep-ph\]](#).
- [77] Adriano Cherkiglia, Dominik Stöckinger, and Hyejung Stöckinger-Kim, “Muon $g-2$ in the 2HDM: maximum results and detailed phenomenology,” *Phys. Rev. D* **98**, 035001 (2018), [arXiv:1711.11567 \[hep-ph\]](#).
- [78] Lei Wang, Jin Min Yang, Mengchao Zhang, and Yang Zhang, “Revisiting lepton-specific 2HDM in light of muon $g - 2$ anomaly,” *Phys. Lett. B* **788**, 519–529 (2019), [arXiv:1809.05857 \[hep-ph\]](#).
- [79] Eung Jin Chun, Jongkuk Kim, and Tanmoy Mondal, “Electron EDM and Muon anomalous magnetic moment in Two-Higgs-Doublet Models,” *JHEP* **12**, 068 (2019), [arXiv:1906.00612 \[hep-ph\]](#).
- [80] Syuhei Iguro, Yuji Omura, and Michihisa Takeuchi, “Testing the 2HDM explanation of the muon $g - 2$ anomaly at the LHC,” *JHEP* **11**, 130 (2019), [arXiv:1907.09845 \[hep-ph\]](#).
- [81] Eung Jin Chun and Tanmoy Mondal, “Searching for a Light Higgs Boson via the Yukawa Process at Lepton Colliders,” *Phys. Lett. B* **802**, 135190 (2020), [arXiv:1909.09515 \[hep-ph\]](#).
- [82] Sudip Jana, Vishnu P. K., and Shaikh Saad, “Resolving electron and muon $g - 2$ within the 2HDM,” *Phys. Rev. D* **101**, 115037 (2020), [arXiv:2003.03386 \[hep-ph\]](#).
- [83] Shao-Ping Li, Xin-Qiang Li, Yuan-Yuan Li, Ya-Dong Yang, and Xin Zhang, “Power-aligned 2HDM: a correlative perspective on $(g - 2)_{e,\mu}$,” *JHEP* **01**, 034 (2021), [arXiv:2010.02799 \[hep-ph\]](#).
- [84] Wai-Yee Keung, Danny Marfatia, and Po-Yan Tseng, “Axion-Like Particles, Two-Higgs-Doublet Models, Leptoquarks, and the Electron and Muon $g - 2$,” *LHEP* **2021**, 209 (2021), [arXiv:2104.03341 \[hep-ph\]](#).
- [85] P. M. Ferreira, B. L. Gonçalves, F. R. Joaquim, and Marc Sher, “ $(g - 2)_\mu$ in the 2HDM and slightly beyond: An updated view,” *Phys. Rev. D* **104**, 053008 (2021), [arXiv:2104.03367 \[hep-ph\]](#).
- [86] Xiao-Fang Han, Tianjun Li, Hong-Xin Wang, Lei Wang, and Yang Zhang, “Lepton-specific inert two-Higgs-doublet model confronted with the new results for muon and electron $g-2$ anomalies and multilepton searches at the LHC,” *Phys. Rev. D* **104**, 115001 (2021), [arXiv:2104.03227 \[hep-ph\]](#).
- [87] Eung Jin Chun and Tanmoy Mondal, “Leptophilic bosons and muon $g-2$ at lepton colliders,” *JHEP* **07**, 044 (2021), [arXiv:2104.03701 \[hep-ph\]](#).
- [88] Adil Jueid, Jinheung Kim, Soojin Lee, and Jeonghyeon Song, “Type-X two-Higgs-doublet model in light of the muon $g-2$: Confronting Higgs boson and collider data,” *Phys. Rev. D* **104**, 095008 (2021), [arXiv:2104.10175 \[hep-ph\]](#).
- [89] Peter Athron, Csaba Balázs, Douglas H. J. Jacob, Wojciech Kotlarski, Dominik Stöckinger, and Hyejung Stöckinger-Kim, “New physics explanations of a_μ in light of the FNAL muon $g - 2$ measurement,” *JHEP* **09**, 080 (2021), [arXiv:2104.03691 \[hep-ph\]](#).
- [90] Wei-Shu Hou and Girish Kumar, “Charged lepton flavor violation in light of muon $g - 2$,” *Eur. Phys. J. C* **81**, 1132 (2021), [arXiv:2107.14114 \[hep-ph\]](#).
- [91] Atri Dey, Jayita Lahiri, and Biswarup Mukhopadhyaya, “Muon $g-2$ and a type-X two Higgs doublet scenario: some studies in high-scale validity,” (2021), [arXiv:2106.01449 \[hep-ph\]](#).
- [92] Wei-Shu Hou, Rishabh Jain, Chung Kao, Girish Kumar, and Tanmoy Modak, “Collider Prospects for Muon $g - 2$ in General Two Higgs Doublet Model,” *Phys. Rev. D* **104**, 075036 (2021), [arXiv:2105.11315 \[hep-ph\]](#).
- [93] Peter Athron, Csaba Balazs, Tomás E. Gonzalo, Douglas Jacob, Farvah Mahmoudi, and Cristian Sierra, “Likelihood analysis of the flavour anomalies and $g - 2$ in the general two Higgs doublet model,” *JHEP* **01**, 037 (2022), [arXiv:2111.10464 \[hep-ph\]](#).
- [94] Andreas Crivellin, Julian Heeck, and Peter Stoffer, “A perturbed lepton-specific two-Higgs-doublet model facing experimental hints for physics beyond the Standard Model,” *Phys. Rev. Lett.* **116**, 081801 (2016), [arXiv:1507.07567 \[hep-ph\]](#).
- [95] Chuan-Hung Chen and Takaaki Nomura, “Charged-Higgs on $R_{D^{(*)}}$, τ polarization, and FBA,” *Eur. Phys. J. C* **77**, 631 (2017), [arXiv:1703.03646 \[hep-ph\]](#).
- [96] Shao-Ping Li, Xin-Qiang Li, Ya-Dong Yang, and Xin Zhang, “ $R_{D^{(*)}}$, $R_{K^{(*)}}$ and neutrino mass in the 2HDM-III with right-handed neutrinos,” *JHEP* **09**, 149 (2018), [arXiv:1807.08530 \[hep-ph\]](#).
- [97] Nivedita Ghosh and Jayita Lahiri, “Revisiting a generalized two-Higgs-doublet model in light of the muon anomaly and lepton flavor violating decays at the HL-LHC,” *Phys. Rev. D* **103**, 055009 (2021), [arXiv:2010.03590 \[hep-ph\]](#).
- [98] Junmou Chen, Qiaoyi Wen, Fanrong Xu, and Mengchao Zhang, “Flavor Anomalies Accommodated in A Flavor Gauged Two Higgs Doublet Model,” (2021), [arXiv:2104.03699 \[hep-ph\]](#).
- [99] Ufuk Aydemir and Tanmoy Mandal, “LHC probes of TeV-scale scalars in SO(10) grand unification,” *Adv. High Energy Phys.* **2017**, 7498795 (2017), [arXiv:1601.06761 \[hep-ph\]](#).
- [100] Rabindra N. Mohapatra and Goran Senjanovic, “The Superlight Axion and Neutrino Masses,” *Z. Phys. C* **17**, 53–56 (1983).
- [101] Jihn E. Kim, “Light Pseudoscalars, Particle Physics and Cosmology,” *Phys. Rept.* **150**, 1–177 (1987).
- [102] Ken Mimasu and Verónica Sanz, “ALPs at Colliders,” *JHEP* **06**, 173 (2015), [arXiv:1409.4792 \[hep-ph\]](#).
- [103] David J. E. Marsh, “Axion Cosmology,” *Phys. Rept.* **643**, 1–79 (2016), [arXiv:1510.07633 \[astro-ph.CO\]](#).
- [104] D. Chang, R. N. Mohapatra, and M. K. Parida, “Decoupling Parity and SU(2)-R Breaking Scales: A New Approach to Left-Right Symmetric Models,” *Phys. Rev. Lett.* **52**, 1072 (1984).
- [105] Alessio Maiezza, Miha Nemevsek, Fabrizio Nesti, and Goran Senjanovic, “Left-Right Symmetry at LHC,” *Phys. Rev. D* **82**, 055022 (2010), [arXiv:1005.5160 \[hep-ph\]](#).

- ph].
- [106] Peter Cox, Alexander Kusenko, Olcyr Sumensari, and Tsutomu T. Yanagida, “SU(5) Unification with TeV-scale Leptoquarks,” *JHEP* **03**, 035 (2017), [arXiv:1612.03923 \[hep-ph\]](#).
 - [107] Jogesh C. Pati and Abdus Salam, “Lepton Number as the Fourth Color,” *Phys. Rev.* **D10**, 275–289 (1974), [Erratum: *Phys. Rev.* D11,703(1975)].
 - [108] G. R. Dvali, “Light color triplet Higgs is compatible with proton stability: An Alternative approach to the doublet - triplet splitting problem,” *Phys. Lett.* **B372**, 113–120 (1996), [arXiv:hep-ph/9511237 \[hep-ph\]](#).
 - [109] Basudeb Dasgupta, Ernest Ma, and Koji Tsumura, “Weakly interacting massive particle dark matter and radiative neutrino mass from Peccei-Quinn symmetry,” *Phys. Rev. D* **89**, 041702 (2014), [arXiv:1308.4138 \[hep-ph\]](#).
 - [110] Sheldon L. Glashow and Steven Weinberg, “Natural Conservation Laws for Neutral Currents,” *Phys. Rev. D* **15**, 1958 (1977).
 - [111] E. A. Paschos, “Diagonal Neutral Currents,” *Phys. Rev. D* **15**, 1966 (1977).
 - [112] Priyotosh Bandyopadhyay and Rusa Mandal, “Vacuum stability in an extended standard model with a leptoquark,” *Phys. Rev. D* **95**, 035007 (2017), [arXiv:1609.03561 \[hep-ph\]](#).
 - [113] S. Navas *et al.* (Particle Data Group), “Review of particle physics,” *Phys. Rev. D* **110**, 030001 (2024).
 - [114] S. Schael *et al.* (SLD Electroweak Group, DELPHI, ALEPH, SLD, SLD Heavy Flavour Group, OPAL, LEP Electroweak Working Group, L3 Collaborations), “Precision electroweak measurements on the Z resonance,” *Phys. Rept.* **427**, 257–454 (2006), [arXiv:hep-ex/0509008 \[hep-ex\]](#).
 - [115] K. Abe *et al.* (Super-Kamiokande Collaboration), “Search for proton decay via $p \rightarrow e^+ \pi^0$ and $p \rightarrow \mu^+ \pi^0$ in 0.31 megaton 7 years exposure of the Super-Kamiokande water Cherenkov detector,” *Phys. Rev. D* **95**, 012004 (2017), [arXiv:1610.03597 \[hep-ex\]](#).
 - [116] Paul Langacker, “Grand Unified Theories and Proton Decay,” *Phys. Rept.* **72**, 185 (1981).
 - [117] J  r  my Bernon, John F. Gunion, Howard E. Haber, Yun Jiang, and Sabine Kraml, “Scrutinizing the alignment limit in two-Higgs-doublet models. II. $m_H=125$ GeV,” *Phys. Rev. D* **93**, 035027 (2016), [arXiv:1511.03682 \[hep-ph\]](#).
 - [118] Philip Bechtle, Daniel Dercks, Sven Heinemeyer, Tobias Klingl, Tim Stefaniak, Georg Weiglein, and Jonas Wittbrodt, “HiggsBounds-5: Testing Higgs Sectors in the LHC 13 TeV Era,” *Eur. Phys. J. C* **80**, 1211 (2020), [arXiv:2006.06007 \[hep-ph\]](#).
 - [119] Shaikh Saad, “Combined explanations of $(g-2)_\mu$, $R_{D^{(*)}}$, $R_{K^{(*)}}$ anomalies in a two-loop radiative neutrino mass model,” *Phys. Rev. D* **102**, 015019 (2020), [arXiv:2005.04352 \[hep-ph\]](#).
 - [120] Georges Aad *et al.* (ATLAS Collaboration), “Search for heavy Higgs bosons decaying into two tau leptons with the ATLAS detector using pp collisions at $\sqrt{s} = 13$ TeV,” *Phys. Rev. Lett.* **125**, 051801 (2020), [arXiv:2002.12223 \[hep-ex\]](#).
 - [121] Arvind Bhaskar, Diganta Das, Tanumoy Mandal, Subhadip Mitra, and Cyrin Neeraj, “Precise limits on the charge-2/3 U1 vector leptoquark,” *Phys. Rev. D* **104**, 035016 (2021), [arXiv:2101.12069 \[hep-ph\]](#).
 - [122] Davide Meloni, Tommy Ohlsson, and Stella Riad, “Effects of intermediate scales on renormalization group running of fermion observables in an SO(10) model,” *JHEP* **12**, 052 (2014), [arXiv:1409.3730 \[hep-ph\]](#).
 - [123] Albert M Sirunyan *et al.* (CMS Collaboration), “Constraints on models of scalar and vector leptoquarks decaying to a quark and a neutrino at $\sqrt{s} = 13$ TeV,” *Phys. Rev. D* **98**, 032005 (2018), [arXiv:1805.10228 \[hep-ex\]](#).
 - [124] Morad Aaboud *et al.* (ATLAS Collaboration), “Searches for third-generation scalar leptoquarks in $\sqrt{s} = 13$ TeV pp collisions with the ATLAS detector,” *JHEP* **06**, 144 (2019), [arXiv:1902.08103 \[hep-ex\]](#).
 - [125] Georges Aad *et al.* (ATLAS Collaboration), “Search for pairs of scalar leptoquarks decaying into quarks and electrons or muons in $\sqrt{s} = 13$ TeV pp collisions with the ATLAS detector,” *JHEP* **10**, 112 (2020), [arXiv:2006.05872 \[hep-ex\]](#).
 - [126] Albert M Sirunyan *et al.* (CMS Collaboration), “Search for singly and pair-produced leptoquarks coupling to third-generation fermions in proton-proton collisions at $\sqrt{s}=13$ TeV,” *Phys. Lett. B* **819**, 136446 (2021), [arXiv:2012.04178 \[hep-ex\]](#).
 - [127] Kushagra Chandak, Tanumoy Mandal, and Subhadip Mitra, “Hunting for scalar leptoquarks with boosted tops and light leptons,” *Phys. Rev. D* **100**, 075019 (2019), [arXiv:1907.11194 \[hep-ph\]](#).
 - [128] Arvind Bhaskar, Tanumoy Mandal, and Subhadip Mitra, “Boosting vector leptoquark searches with boosted tops,” *Phys. Rev. D* **101**, 115015 (2020), [arXiv:2004.01096 \[hep-ph\]](#).
 - [129] Arvind Bhaskar, Tanumoy Mandal, Subhadip Mitra, and Mohit Sharma, “Improving third-generation leptoquark searches with combined signals and boosted top quarks,” *Phys. Rev. D* **104**, 075037 (2021), [arXiv:2106.07605 \[hep-ph\]](#).
 - [130] Arvind Bhaskar, Yash Chaurasia, Kuldeep Deka, Tanumoy Mandal, Subhadip Mitra, and Ananya Mukherjee, “Right-handed neutrino pair production via second-generation leptoquarks,” *Phys. Lett. B* **843**, 138039 (2023), [arXiv:2301.11889 \[hep-ph\]](#).
 - [131] Murad Ali, Shaaban Khalil, Stefano Moretti, Shoaib Munir, Roman Nevzorov, Alexandre Nikitenko, and Harri Waltari, “TeV-scale leptoquark searches at the LHC and their E_6 SSM interpretation,” *JHEP* **03**, 117 (2023), [arXiv:2302.02071 \[hep-ph\]](#).
 - [132] Georges Aad *et al.* (ATLAS Collaboration), “Search for excited τ -leptons and leptoquarks in the final state with τ -leptons and jets in pp collisions at $\sqrt{s} = 13$ TeV with the ATLAS detector,” *JHEP* **06**, 199 (2023), [arXiv:2303.09444 \[hep-ex\]](#).
 - [133] Aram Hayrapetyan *et al.* (CMS Collaboration), “Search for Scalar Leptoquarks Produced via τ -Lepton-Quark Scattering in pp Collisions at $\sqrt{s}=13$ TeV,” *Phys. Rev. Lett.* **132**, 061801 (2024), [arXiv:2308.06143 \[hep-ex\]](#).
 - [134] Arvind Bhaskar, Arijit Das, Tanumoy Mandal, Subhadip Mitra, and Rachit Sharma, “Fresh look at the LHC limits on scalar leptoquarks,” *Phys. Rev. D* **109**, 055018 (2024), [arXiv:2312.09855 \[hep-ph\]](#).
 - [135] Georges Aad *et al.* (ATLAS Collaboration), “Combination of searches for pair-produced leptoquarks at $\sqrt{s}=13$

- TeV with the ATLAS detector,” *Phys. Lett. B* **854**, 138736 (2024), [arXiv:2401.11928 \[hep-ex\]](#).
- [136] Armen Tumasyan *et al.* (CMS Collaboration), “Inclusive nonresonant multilepton probes of new phenomena at $\sqrt{s}=13$ TeV,” *Phys. Rev. D* **105**, 112007 (2022), [arXiv:2202.08676 \[hep-ex\]](#).
- [137] Celine Degrande, Claude Duhr, Benjamin Fuks, David Grellscheid, Olivier Mattelaer, and Thomas Reiter, “UFO - The Universal FeynRules Output,” *Comput. Phys. Commun.* **183**, 1201–1214 (2012), [arXiv:1108.2040 \[hep-ph\]](#).
- [138] J. Alwall, R. Frederix, S. Frixione, V. Hirschi, F. Maltoni, O. Mattelaer, H. S. Shao, T. Stelzer, P. Torrielli, and M. Zaro, “The automated computation of tree-level and next-to-leading order differential cross sections, and their matching to parton shower simulations,” *JHEP* **07**, 079 (2014), [arXiv:1405.0301 \[hep-ph\]](#).
- [139] Richard D. Ball *et al.*, “Parton distributions with LHC data,” *Nucl. Phys. B* **867**, 244–289 (2013), [arXiv:1207.1303 \[hep-ph\]](#).
- [140] Tanumoy Mandal, Subhadip Mitra, and Satyajit Seth, “Pair Production of Scalar Leptoquarks at the LHC to NLO Parton Shower Accuracy,” *Phys. Rev. D* **93**, 035018 (2016), [arXiv:1506.07369 \[hep-ph\]](#).
- [141] Tanumoy Mandal and Subhadip Mitra, “Probing Color Octet Electrons at the LHC,” *Phys. Rev. D* **87**, 095008 (2013), [arXiv:1211.6394 \[hep-ph\]](#).
- [142] Tanumoy Mandal, Subhadip Mitra, and Satyajit Seth, “Single Productions of Colored Particles at the LHC: An Example with Scalar Leptoquarks,” *JHEP* **07**, 028 (2015), [arXiv:1503.04689 \[hep-ph\]](#).
- [143] Tanumoy Mandal, Subhadip Mitra, and Satyajit Seth, “Probing Compositeness with the CMS $eejj$ & eej Data,” *Phys. Lett. B* **758**, 219–225 (2016), [arXiv:1602.01273 \[hep-ph\]](#).
- [144] J. Grygier *et al.* (Belle Collaboration), “Search for $B \rightarrow h\nu\bar{\nu}$ decays with semileptonic tagging at Belle,” *Phys. Rev. D* **96**, 091101 (2017), [Addendum: *Phys. Rev. D* **97**, 099902 (2018)], [arXiv:1702.03224 \[hep-ex\]](#).
- [145] Y. Amhis *et al.* (HFLAV Collaboration), “Averages of b -hadron, c -hadron, and τ -lepton properties as of summer 2016,” *Eur. Phys. J. C* **77**, 895 (2017), [arXiv:1612.07233 \[hep-ex\]](#).
- [146] Roel Aaij *et al.* (LHCb Collaboration), “Measurement of the $B_s^0 \rightarrow \mu^+\mu^-$ branching fraction and effective lifetime and search for $B^0 \rightarrow \mu^+\mu^-$ decays,” *Phys. Rev. Lett.* **118**, 191801 (2017), [arXiv:1703.05747 \[hep-ex\]](#).
- [147] F. Staub, “SARAH,” (2008), [arXiv:0806.0538 \[hep-ph\]](#).
- [148] Florian Staub, “SARAH 4 : A tool for (not only SUSY) model builders,” *Comput. Phys. Commun.* **185**, 1773–1790 (2014), [arXiv:1309.7223 \[hep-ph\]](#).
- [149] Mark D. Goodsell, Kilian Nickel, and Florian Staub, “Two-Loop Higgs mass calculations in supersymmetric models beyond the MSSM with SARAH and SPheno,” *Eur. Phys. J. C* **75**, 32 (2015), [arXiv:1411.0675 \[hep-ph\]](#).
- [150] M. Goodsell, K. Nickel, and F. Staub, “Generic two-loop Higgs mass calculation from a diagrammatic approach,” *Eur. Phys. J. C* **75**, 290 (2015), [arXiv:1503.03098 \[hep-ph\]](#).
- [151] Florian Staub, “Exploring new models in all detail with SARAH,” *Adv. High Energy Phys.* **2015**, 840780 (2015), [arXiv:1503.04200 \[hep-ph\]](#).
- [152] Mark D. Goodsell and Florian Staub, “The Higgs mass in the CP violating MSSM, NMSSM, and beyond,” *Eur. Phys. J. C* **77**, 46 (2017), [arXiv:1604.05335 \[hep-ph\]](#).
- [153] Johannes Braathen, Mark D. Goodsell, and Florian Staub, “Supersymmetric and non-supersymmetric models without catastrophic Goldstone bosons,” *Eur. Phys. J. C* **77**, 757 (2017), [arXiv:1706.05372 \[hep-ph\]](#).
- [154] Werner Porod, “SPheno, a program for calculating supersymmetric spectra, SUSY particle decays and SUSY particle production at e^+e^- colliders,” *Comput. Phys. Commun.* **153**, 275–315 (2003), [arXiv:hep-ph/0301101](#).
- [155] W. Porod and F. Staub, “SPheno 3.1: Extensions including flavour, CP-phases and models beyond the MSSM,” *Comput. Phys. Commun.* **183**, 2458–2469 (2012), [arXiv:1104.1573 \[hep-ph\]](#).
- [156] Anjan S. Joshipura and Ketan M. Patel, “Fermion Masses in $SO(10)$ Models,” *Phys. Rev. D* **83**, 095002 (2011), [arXiv:1102.5148 \[hep-ph\]](#).
- [157] Davide Meloni, Tommy Ohlsson, and Stella Riad, “Renormalization Group Running of Fermion Observables in an Extended Non-Supersymmetric $SO(10)$ Model,” *JHEP* **03**, 045 (2017), [arXiv:1612.07973 \[hep-ph\]](#).
- [158] D. R. T. Jones, “The Two Loop beta Function for a $G(1) \times G(2)$ Gauge Theory,” *Phys. Rev. D* **25**, 581 (1982).
- [159] M. Lindner and M. Weiser, “Gauge coupling unification in left-right symmetric models,” *Phys. Lett. B* **383**, 405–414 (1996), [arXiv:hep-ph/9605353 \[hep-ph\]](#).
- [160] Marie E. Machacek and Michael T. Vaughn, “Two Loop Renormalization Group Equations in a General Quantum Field Theory. 2. Yukawa Couplings,” *Nucl. Phys. B* **236**, 221–232 (1984).